Available online at http://scik.org
Commun. Math. Biol. Neurosci. 2026, 2026:120
https://doi.org/10.28919/cmbn/10219
ISSN: 2052-2541

MATHEMATICAL MODELING AND OPTIMAL CONTROL OF PROSTATE CANCER DYNAMICS USING CAPUTO FRACTIONAL-ORDER DERIVATIVES

LHOUSSAIN BOUISSOUI[1,*], MUSTAPHA AIT HAMMOU[1], RACHID BOUAJAJI[2]

[1]Laboratory for Modeling, Applied Mathematics and Intelligent Systems (M.M.A.S.I.),
Faculty of Sciences Dhar El Mahraz, Sidi Mohamed Ben Abdellah University, Fez 30003, Morocco
[2]Nursing, Higher Institute of Nursing and Health Care Professions, Meknes, Morocco

Copyright © 2026 the author(s). This is an open access article distributed under the Creative Commons Attribution License, which permits unrestricted use, distribution, and reproduction in any medium, provided the original work is properly cited.

Abstract. This paper develops a fractional-order mathematical model, formulated in the Caputo sense, for the dynamics of prostate cancer (PC) under combined androgen deprivation therapy (ADT) and dendritic-cell (DC)-based immunotherapy. The model extends classical integer-order formulations by incorporating memory effects that reflect the cumulative, history-dependent nature of tumor–immune interactions. Two malignant cell populations are considered — androgen-dependent (AD) and androgen-independent (AI) prostate cancer cells — together with an effector-cell compartment representing the immune response, and auxiliary state variables for circulating androgen level and administered immunotherapeutic agent. We establish positivity and boundedness of solutions, existence and uniqueness via the Banach and Leray–Schauder fixed-point theorems (with full proofs), Ulam–Hyers and Ulam–Hyers–Rassias stability, and a local stability analysis of the model's equilibria via the Matignon stability criterion. Building on this qualitative foundation, we introduce two time-dependent control functions representing the intensity of ADT and the dosage of immunotherapy and formulate an optimal control problem minimizing tumor burden and treatment cost over a finite horizon. Necessary optimality conditions are derived via a fractional-order Pontryagin Maximum Principle, and the resulting boundary value problem is solved with a forward–backward sweep scheme coupled to a fractional Euler / product-integration method; a local truncation error analysis, a formal global error estimate, and a local step-size stability heuristic are derived for this scheme,

*Corresponding author
E-mail address: lhoussain.bouissoui@usmba.ac.ma
Received August 12, 2026

and reconciled with the full-memory quadrature actually implemented via the standard convergence theory of fractional Adams-type methods. This numerical scheme is validated to full convergence on a short time horizon, while on the longer horizon used for the main simulations the co-state sweep is numerically stiff (a consequence of the model's own unconditionally unstable growth mode) and the reported long-horizon control profile is accordingly presented as an illustrative profile consistent with the derived optimality conditions rather than as a fully converged numerical solution. Numerical simulations, carried out in Python for several values of the fractional order δ and for several values of the competition and killing-rate parameters α, β, and a_2, illustrate how memory effects and inter-cell competition shape the transient and long-run behavior of the model, and a qualitative sensitivity analysis characterizes the relative influence of each parameter on tumor burden. The results indicate that fractional-order optimal control provides a flexible, biologically motivated framework for exploring individualized combination therapies for prostate cancer, while also highlighting a trade-off between aggressive androgen suppression and the emergence of androgen-independent, treatment-resistant disease.

Keywords: prostate cancer; Caputo fractional derivative; optimal control; Pontryagin maximum principle; immunotherapy; androgen deprivation therapy; Ulam–Hyers stability; fractional Euler method.

2020 AMS Subject Classification: 26A33; 34A08; 49K15; 92C50.

1. INTRODUCTION

Prostate cancer (PC) remains one of the most commonly diagnosed malignancies in men worldwide, and its clinical management is complicated by the tumor's capacity to transition from an androgen-dependent (AD) phenotype, which is sensitive to androgen deprivation therapy (ADT), to an androgen-independent (AI) phenotype associated with castration resistance [1, 2, 3]. Testosterone and its metabolite 5α-dihydrotestosterone (DHT) play a central role in prostate cell proliferation: while essential for normal prostate development, these androgens also stimulate the growth of PC cells and inhibit apoptosis. Androgen suppression has therefore become a cornerstone of clinical management, administered either as continuous androgen deprivation (CAD), involving uninterrupted drug administration, or as intermittent androgen deprivation (IAD), in which treatment is cyclically suspended and resumed according to prostate-specific antigen (PSA) thresholds [4, 5].

A persistent clinical challenge is that ADT, while effective at controlling AD disease, exerts selective pressure that can favor the emergence and expansion of AI cell populations, which no longer depend on androgen signaling for survival and proliferation and are consequently resistant to hormonal therapy [6, 7]. This has motivated growing interest in combination therapies

that pair ADT with immunotherapy, which harnesses the patient's own immune system to target cancer cells regardless of androgen dependence [8, 9]. Dendritic cells (DCs), highly effective antigen-presenting cells, play a central role in initiating such immunotherapeutic responses: by loading autologous DCs with tumor antigen and re-injecting them, a DC-based vaccine can activate naive T cells and disrupt peripheral immune tolerance, producing a tumor-specific immune reaction [10]. Clinical trials of DC-based vaccines have shown heterogeneous responses, with some patients experiencing marked PSA reductions and others showing continued disease progression, underscoring the need for a quantitative, model-based understanding of how the timing and intensity of combined ADT and immunotherapy shape the joint dynamics of AD cells, AI cells, and the immune response.

1.1. Mathematical models of prostate cancer. Mathematical modeling has played an increasingly important role in understanding the dynamics of the AD-to-AI transition and in guiding the design of treatment schedules. Rutter and Kuang [1] formulated a system of ordinary differential equations coupling AD and AI cell populations, an effector-cell compartment, circulating androgen, and a DC-vaccine state variable, and analyzed its global dynamics under joint hormone and immunotherapy. This model was subsequently extended to incorporate pulsed dosing schedules and stochastic perturbations [11], and related models have examined sliding-mode and other feedback control strategies for androgen suppression [5]. These integer-order models have provided valuable qualitative insight — in particular, they capture the characteristic non-monotonic evolution of AD and AI populations under treatment, and the possibility of relapse into a castration-resistant state.

1.2. Fractional calculus in biological modeling. While integer-order ordinary differential equation (ODE) models have provided valuable qualitative insight into PC dynamics under treatment, they inherently assume that the system's evolution depends only on its present state, and therefore cannot capture memory or hereditary effects that are widely believed to be present in biological and physiological processes. Fractional calculus, which studies derivatives and integrals of non-integer order, offers a natural mathematical framework for incorporating such memory effects, since the fractional derivative at a given time depends (through a weighted integral) on the entire history of the state variable rather than on its instantaneous rate of change

alone [12, 13, 14, 15]. This property has motivated a rapidly growing literature applying fractional operators to tumor–immune dynamics, epidemic models, and other biological and physiological systems [16, 17, 18, 19, 20, 21, 22, 23, 24]. In particular, a Caputo fractional-order version of the Rutter–Kuang pulsed-treatment model was recently developed and analyzed by Saber et al. [25], who established existence, uniqueness, and Ulam–Hyers stability of solutions and investigated, via the fractional Euler method, the influence of the fractional order and of inter-cell competition and killing-rate parameters on the qualitative dynamics of the model. The present paper builds directly on this fractional-order formulation.

Very recent work continues to extend this line of research to other cancer types and other fractional operators. Salah et al. [26] developed a fractal-fractional model of stem-cell/chemotherapy combinations, and a fractional-order lung cancer model incorporating time-delayed internal influences was proposed in [27]; a fractional-order cancer biomarker model, coupled with particle swarm optimization for parameter and nanoparticle-dosage estimation, was analyzed in [28]; and a Caputo fractional spatiotemporal extension of the classical Hahnfeldt tumor-angiogenesis model, with an accompanying convergence analysis, was presented in [29]. Fractional and variable-order models specifically incorporating optimal control have also been developed for breast cancer [30, 31] and, using the Atangana–Baleanu–Caputo operator, for a general multi-compartment cancer-treatment model [32]; most recently, Ramalakshmi and Samei [33] formulated a Caputo fractional optimal-control model for endometrial cancer under combined immunotherapy (dostarlimab) and chemotherapy, closely paralleling in structure, though for a different cancer type, the combined hormonal/immunotherapy optimal control problem formulated in Section 6 below. These studies collectively confirm both the timeliness and the methodological generality of combining fractional-order modeling with optimal control theory for cancer treatment design, and several of their techniques (variable-order operators, fractal-fractional kernels, delay terms) are natural candidates for future extensions of the present model, as discussed in Section 9.

1.3. From qualitative analysis to optimal control. A further modeling gap concerns treatment optimization. Existing fractional-order PC models, including [25], have largely focused on qualitative analysis (existence, uniqueness, and stability of solutions) and on simulating

the system's response to fixed, pre-specified pulsed treatment protocols, rather than on determining treatment protocols that are optimal with respect to a clinically meaningful objective. Optimal control theory provides the natural mathematical machinery for this task: given a model of tumor–immune dynamics and a set of admissible control inputs (e.g., the intensity of ADT and the dosage of immunotherapy), one seeks the control strategy that minimizes a cost functional balancing tumor burden against the side effects and cost of treatment. Fractional-order optimal control has recently been applied to other cancer and infectious-disease models [34, 35, 36, 32, 33, 30, 31], and, on the integer-order side, mechanistic and quantitative-systems-pharmacology (QSP) models have specifically examined the scheduling and combination of ADT with dendritic-cell and checkpoint-blockade immunotherapy for prostate cancer [37, 38], as well as game-theoretic extensions of the classical Baez–Kuang ODE framework for castration-resistant disease [39]. However, to the best of our knowledge, few if any studies have combined fractional-order optimal control with the pulsed-treatment prostate cancer framework of [1, 25], which is the specific gap addressed by the present paper.

1.4. Contributions and organization. Motivated by these considerations, the present paper makes the following contributions:

(i) We formulate a Caputo fractional-order model of PC dynamics that extends the pulsed-treatment model of [25] by introducing two time-dependent control functions representing the intensity of ADT and the dosage rate of DC-based immunotherapy.

(ii) We establish positivity and boundedness of solutions, and prove existence and uniqueness of solutions of the controlled system using the Banach and Leray–Schauder fixed-point theorems, giving full proofs rather than sketches.

(iii) We examine Ulam–Hyers, generalized Ulam–Hyers, Ulam–Hyers–Rassias, and generalized Ulam–Hyers–Rassias stability of the controlled model.

(iv) We analyze the equilibria of the uncontrolled model and their local asymptotic stability via a fractional-order linearization and the Matignon stability criterion.

(v) We formulate an optimal control problem whose cost functional penalizes both AD and AI cell burden and the cost of the two control inputs, and we derive necessary optimality conditions via a fractional-order Pontryagin Maximum Principle.

(vi) We develop a numerical scheme, combining a forward–backward sweep method with a fractional Euler / product-integration method, analyze its local truncation error, a formal global error estimate, and a local step-size stability heuristic, and implement it in Python.

(vii) We present numerical simulations — including a sensitivity analysis with respect to the fractional order δ and the parameters α, β, and a_2 — illustrating the qualitative and quantitative behavior of the controlled and uncontrolled model.

The remainder of the paper is organized as follows. Section 2 recalls the necessary preliminaries of Caputo fractional calculus. Section 3 introduces the controlled fractional-order PC model and its basic properties. Section 4 establishes existence, uniqueness, and Ulam–Hyers-type stability results. Section 5 analyzes the model's equilibria and their local stability. Section 6 formulates the optimal control problem and derives the necessary optimality conditions. Section 7 describes the numerical scheme and its convergence analysis. Section 8 presents and discusses the numerical simulations. Section 9 concludes the paper and outlines directions for future work. Appendix A collects additional derivations, and Appendix B summarizes the numerical implementation.

2. PRELIMINARIES

We first recall standard definitions and results from fractional calculus that will be used throughout the paper.

Definition 2.1 (Caputo fractional derivative)**.** *For a function $H \in C^1([0,T],\mathbb{R})$ and fractional order $\delta \in (0,1)$, the Caputo fractional derivative is defined as*

$$ {}^{C}D_t^{\delta} H(t) = \frac{1}{\Gamma(1-\delta)} \int_0^t (t-\varpi)^{-\delta} \frac{d}{d\varpi} H(\varpi)\, d\varpi. $$

For the boundary case $\delta = 1$, the formula above is not directly applicable (the kernel $\Gamma(1-\delta)^{-1}(t-\varpi)^{-\delta}$ is undefined at $\delta = 1$, since $\Gamma(0)$ is infinite); by convention, and consistently with the limit $\delta \to 1^-$ of the fractional-integral representation, one instead defines *${}^{C}D_t^{1} H(t) := H'(t)$, the classical first derivative. All results in this paper stated for $\delta \in (0,1]$ are understood*

in this sense, with $\delta = 1$ recovering the classical (integer-order) model as a genuine special case rather than a limiting approximation.

Definition 2.2 (Riemann–Liouville fractional integral)**.** *For $H \in L^1([0,T],\mathbb{R})$,*

$$I^{\delta}H(t) = \frac{1}{\Gamma(\delta)}\int_0^t (t-\varpi)^{\delta-1}H(\varpi)\,d\varpi.$$

Remark 2.1. *Unlike the classical integer-order derivative, ${}^{C}D_t^{\delta}H(t)$ depends on the values of H over the entire interval $[0,t]$ rather than only in an infinitesimal neighbourhood of t; this non-local, weighted-history dependence is commonly referred to as a* memory effect. *As $\delta \to 1^{-}$, the Caputo derivative recovers the classical first derivative, $H'(t)$, so that the fractional model reduces continuously to the underlying integer-order model of* [1] *in this limit.*

Definition 2.3 (Mittag–Leffler function)**.** *For $\beta > 0$ and $z \in \mathbb{C}$, the one-parameter Mittag–Leffler function is*

$$E_{\beta}(z) = \sum_{k=0}^{\infty} \frac{z^k}{\Gamma(\beta k+1)}.$$

It plays the role for fractional-order linear systems that the exponential function plays for integer-order linear systems.

Theorem 2.1 (Banach fixed-point theorem)**.** *Let $\mathscr{F}$ be a Banach space and $B \subset \mathscr{F}$ a nonempty closed set. If $W : B \to B$ is a contraction, i.e., there exists $\kappa \in [0,1)$ such that $\|WP_1 - WP_2\| \leq \kappa\|P_1 - P_2\|$ for all $P_1, P_2 \in B$, then W admits a unique fixed point in B.*

Theorem 2.2 (Leray–Schauder / Schauder alternative)**.** *Let $\mathscr{F}$ be a Banach space and $W : \mathscr{F} \to \mathscr{F}$ a completely continuous operator (continuous and mapping bounded sets to relatively compact sets). Then either*

(a) W has a fixed point, or

(b) the set $\{P \in \mathscr{F} : P = \lambda WP \text{ for some } \lambda \in (0,1)\}$ is unbounded.

Theorem 2.3 (Arzelà–Ascoli theorem)**.** *A subset S of $C([0,T],\mathbb{R}^n)$ is relatively compact if and only if S is uniformly bounded and equicontinuous.*

Theorem 2.4 (Generalized Grönwall inequality [40]). *Let $x(t)$ be a nonnegative, locally integrable function on $[0,T)$ and suppose*

$$x(t) \le a(t) + b\int_0^t (t-s)^{\beta-1} x(s)\,ds,$$

where $a(t)$ is nondecreasing, $b \ge 0$, and $\beta > 0$. Then

$$x(t) \le a(t)\,E_\beta\big(b\,\Gamma(\beta)\,t^\beta\big).$$

Theorem 2.5 (Matignon stability criterion). *Consider the linear fractional-order system ${}^C D_t^\delta \mathbf{x}(t) = M\mathbf{x}(t)$, $\delta \in (0,1)$, $M \in \mathbb{R}^{n\times n}$. The zero equilibrium is locally asymptotically stable if and only if all eigenvalues λ_i of M satisfy*

$$|\arg(\lambda_i)| > \frac{\delta\pi}{2}.$$

3. The Controlled Fractional-Order Prostate Cancer Model

3.1. Model formulation.

We extend the pulsed-treatment PC model of Rutter and Kuang [1] and its fractional generalization [25] by replacing the fixed treatment terms with two admissible, bounded, Lebesgue-measurable control functions:

- $u_1(t) \in [0, u_1^{\max}]$, $u_1^{\max} \le 1$: intensity of androgen deprivation therapy at time t, driving the target androgen level toward $a_0(1-u_1(t))$;
- $u_2(t) \in [0, u_2^{\max}]$: dosage rate of DC-based immunotherapy at time t, representing the rate at which antigen-loaded dendritic cells are infused.

The controlled fractional-order model, formulated with the Caputo derivative of order $\delta \in (0,1]$, reads:

$$\begin{aligned}
{}^C D_t^\delta X_1 &= X_1\left[e_1 A\left(1-\tfrac{X_1+\alpha X_2}{Q}\right) - (d_1+m_1)\left(1-\tfrac{A}{a_0}\right) \right.\\
&\qquad \left. -\tfrac{a_1 Y}{g_1+X_1+X_2}\right],\\
{}^C D_t^\delta X_2 &= e_2\left(1-\tfrac{\beta X_1+X_2}{Q}\right)X_2 + m_1\left(1-\tfrac{A}{a_0}\right)X_1\\
&\qquad -\tfrac{a_2 X_2 Y}{g_2+X_1+X_2},\\
{}^C D_t^\delta Y &= (W-\omega)Y + \tfrac{\varepsilon \mathscr{J}}{g_3+\mathscr{J}},\\
{}^C D_t^\delta A &= -\gamma\big(A - a_0(1-u_1(t))\big),
\end{aligned} \tag{1}$$

$$
\begin{aligned}
{}^{C}D_t^{\delta}\mathscr{J} \qquad\qquad &= -c\,\mathscr{J} + u_2(t),
\end{aligned}
$$

subject to non-negative initial conditions $X_1(0) = X_{10} \geq 0$, $X_2(0) = X_{20} \geq 0$, $Y(0) = Y_0 \geq 0$, $A(0) = A_0 \geq 0$, $\mathscr{J}(0) = \mathscr{J}_0 \geq 0$.

Here X_1 and X_2 denote the AD and AI prostate cancer cell populations, Y the effector (immune) cell population, A the serum androgen level, and $\mathscr{J}$ the level of activated antigen-presenting dendritic cells. The parameter Q is the shared carrying capacity, α and β quantify inter-population competition (of AI cells on AD cells, and of AD cells on AI cells, respectively), d_1 is the AD death rate, m_1 the (irreversible) mutation rate from AD to AI phenotype, a_1, a_2 the maximal effector-cell killing rates of AD and AI cells respectively, g_1, g_2 the corresponding half-saturation constants, W the maximal effector-cell stimulation rate, ω the effector-cell death rate, ε the maximal antigen-driven stimulation rate, g_3 the DC saturation constant, γ the androgen clearance rate, a_0 the pre-treatment androgen level, and c the DC decay rate. Setting $u_1 \equiv u_2 \equiv 0$ recovers the untreated fractional model of [25], while constant or pulsed choices of u_1, u_2 recover CAD/IAD and DC-vaccine pulse protocols previously studied in the literature.

Remark 3.1. *Every term of the X_1 equation is proportional to X_1, exactly mirroring the multiplicative (logistic-type) structure already present in the X_2 equation. This is the natural population-dynamics convention — a cell population with zero individuals contributes zero net flux regardless of the surrounding environment — and it is what makes $\{X_1 = 0\}$ an invariant boundary of the state space, which in turn is what allows the positivity result of Proposition 1 below to be established rigorously rather than merely as a numerically enforced safeguard.*

3.2. Fixed-point reformulation. As in the reference model, system (2) is written in fixed-point form: letting $\mathscr{P}(t) = (X_1, X_2, Y, A, \mathscr{J})^{\top}$ and $\mathscr{U}(t, \mathscr{P}(t))$ the corresponding right-hand-side vector field (with the control functions treated as fixed, given inputs), applying the fractional integral operator I^{δ} to both sides of (2) and using the fact that $I^{\delta}\,{}^{C}D_t^{\delta}\mathscr{P}(t) = \mathscr{P}(t) - \mathscr{P}(0)$ for $\mathscr{P} \in C^1$, the system is equivalent to the integral equation

$$
\mathscr{P}(t) = \mathscr{P}_0 + \frac{1}{\Gamma(\delta)} \int_0^t (t - \varpi)^{\delta - 1} \mathscr{U}(\varpi, \mathscr{P}(\varpi))\, d\varpi. \tag{2}
$$

3.3. Positivity and boundedness.

Proposition 1 (Positivity)**.** *Let u_1, u_2 be admissible controls. If $\mathscr{P}_0 \in \mathbb{R}^5_{\geq 0}$, then the corresponding solution $\mathscr{P}(t)$ of* (2) *satisfies $\mathscr{P}(t) \in \mathbb{R}^5_{\geq 0}$ for all $t \geq 0$ where it exists.*

Proof. It suffices to check that on each coordinate hyperplane $\{\mathscr{P}_i = 0\}$ $(i = 1, \ldots, 5)$, the corresponding component of the vector field $\mathscr{U}$ is nonnegative; by the fractional-order extension of the classical Nagumo invariance criterion established by Lin [41] (Theorem 3.1 therein: a closed region is positively invariant for a Caputo fractional-order system provided the vector field is subtangential, i.e. non-outward-pointing, at every boundary point, exactly as in the classical integer-order Nagumo theorem), this is sufficient to prevent trajectories from leaving $\mathbb{R}^5_{\geq 0}$. Indeed:

- At $X_1 = 0$: $\mathscr{U}_1|_{X_1=0} = 0$ *identically*, since every term of $\mathscr{U}_1$ carries an explicit factor of X_1 (Remark 3.1). Hence $\{X_1 = 0\}$ is not merely non-repelling but exactly invariant: once X_1 reaches zero it remains zero for all subsequent time (under the stated non-negativity of A, established below), and in particular can never become negative. This is a genuine boundary identity, not merely a bound, and requires no auxiliary hypothesis on the sign of the bracketed factor.
- At $X_2 = 0$: $\mathscr{U}_2|_{X_2=0} = m_1(1 - A/a_0)X_1 \geq 0$ since $A \leq a_0$ (by the boundedness argument of Proposition 2, which does not depend on positivity and may be verified independently) and $X_1 \geq 0$.
- At $Y = 0$: $\mathscr{U}_3|_{Y=0} = \varepsilon \mathscr{J} / (g_3 + \mathscr{J}) \geq 0$.
- At $A = 0$: $\mathscr{U}_4|_{A=0} = \gamma a_0(1 - u_1(t)) \geq 0$ since $u_1(t) \leq 1$.
- At $\mathscr{J} = 0$: $\mathscr{U}_5|_{\mathscr{J}=0} = u_2(t) \geq 0$.

Hence the vector field points into (or exactly along) the boundary of $\mathbb{R}^5_{\geq 0}$ everywhere on the boundary, and $\mathbb{R}^5_{\geq 0}$ is a positively invariant region for (2). (The non-negativity projection $\max(\cdot, 0)$ retained in the numerical scheme of Section 7 is accordingly a pure numerical safeguard against floating-point round-off at the $X_1 = 0$ and $X_2 = 0$ boundaries, not a substitute for this analytical argument.)

□

Proposition 2 (Boundedness)**.** *Under admissible controls, all state variables of* (2) *remain bounded on any finite interval* $[0,T]$*; moreover* $A(t)$ *is bounded uniformly in* t *by* $\max(A_0,a_0)$*, and* X_1+X_2 *is bounded above by a constant depending on* Q,α,β *and the initial data.*

Proof. Since $0 \le u_1(t) \le 1$, the target level $a_0(1-u_1(t)) \in [0,a_0]$; the linear fractional relaxation ${}^{C}D_t^{\delta} A = -\gamma(A - a_0(1-u_1(t)))$ then implies, by a fractional comparison argument, that $A(t)$ remains within the convex hull of A_0 and $[0,a_0]$, i.e. $A(t) \le \max(A_0,a_0)$ for all $t \ge 0$. For the tumor compartments, when X_1+X_2 approaches $Q/\min(1,\alpha,\beta)$ the logistic-type terms $e_1 A(1-(X_1+\alpha X_2)/Q)$ and $e_2(1-(\beta X_1+X_2)/Q)X_2$ become non-positive, while the killing terms $-a_1 Y X_1/(g_1+X_1+X_2)$ and $-a_2 X_2 Y/(g_2+X_1+X_2)$ are non-positive; hence X_1+X_2 cannot grow without bound, and a standard fractional-order argument (using the sub-linear growth condition of Assumption 1 below) yields boundedness of Y and $\mathscr{J}$ on any finite horizon. □

These two propositions confirm that the model is biologically well-posed: cell populations, androgen level, and DC level remain non-negative and bounded, as required for a meaningful interpretation of $\mathscr{P}(t)$.

4. Existence, Uniqueness, and Stability

We work in the Banach space $\mathscr{F} = C([0,T],\mathbb{R}^5)$ with norm $\|\mathscr{P}\| = \sup_{t\in[0,T]} |\mathscr{P}(t)|$, where $|\cdot|$ denotes, as in [25], the sum of absolute values of the components. We define the solution operator $\mathscr{W} : \mathscr{F} \to \mathscr{F}$ by

$$(\mathscr{W}\mathscr{P})(t) = \mathscr{P}_0 + \frac{1}{\Gamma(\delta)} \int_0^t (t-\varpi)^{\delta-1} \mathscr{U}(\varpi, \mathscr{P}(\varpi))\, d\varpi. \tag{3}$$

A fixed point of $\mathscr{W}$ is precisely a solution of the integral equation (2), hence of the controlled model (2).

H 1. *There exist* $\alpha_{\mathscr{U}}, \beta_{\mathscr{U}} > 0$ *such that* $|\mathscr{U}(t,\mathscr{P})| \le \alpha_{\mathscr{U}} |\mathscr{P}| + \beta_{\mathscr{U}}$ *for all* $t \in [0,T]$, $\mathscr{P} \in \mathscr{F}$*, uniformly in the admissible controls* u_1, u_2*.*

H 2. *There exists* $\hbar_{\mathscr{U}} > 0$ *such that* $|\mathscr{U}(t,\mathscr{P}_1) - \mathscr{U}(t,\mathscr{P}_2)| \le \hbar_{\mathscr{U}} |\mathscr{P}_1 - \mathscr{P}_2|$ *for all* $t \in [0,T]$*,* $\mathscr{P}_1, \mathscr{P}_2 \in \mathscr{F}$*, uniformly in the admissible controls.*

Remark 4.1. *On the bounded, positively invariant region identified in Propositions 1–2, the right-hand side $\mathscr{U}$ of* (2) *is continuously differentiable in $\mathscr{P}$ (all denominators $g_1+X_1+X_2$, $g_2+X_1+X_2$, and $g_3+\mathscr{J}$ remain bounded away from zero since $g_1,g_2,g_3>0$), so both Assumption 1 and Assumption 2 hold with $\alpha_{\mathscr{U}},\hbar_{\mathscr{U}}$ given by suitable bounds on the partial derivatives of $\mathscr{U}$ over that region.*

4.1. Existence of a solution. Before stating the results, it is worth clarifying why both an existence theorem (Schauder/Leray–Schauder, Theorem 4.1 below) and a separate uniqueness theorem (Banach, Theorem 4.2) are needed, rather than a single Banach-type argument: existence under Assumption 1 (a sub-linear growth bound) holds on a possibly large ball B_r^* without requiring $\mathscr{U}$ to be a contraction there, whereas uniqueness requires the strictly stronger Lipschitz condition of Assumption 2 together with the smallness condition $\hbar_{\mathscr{U}}T^{\delta}/\Gamma(\delta+1)<1$, which may fail to hold on all of B_r^* (e.g. for large T) even when it holds locally. Schauder's theorem (via compactness, not contraction) therefore secures existence under the weaker hypothesis, while Banach's theorem is invoked separately, under the stronger hypothesis, to secure uniqueness and the constructive Picard iteration of Corollary 4.1 below; this is the standard division of labor between the two theorems in fractional-order fixed-point analysis, and is not redundant.

Theorem 4.1 (Existence)**.** *Under Assumption 1, if there exists $r>0$ such that*

$$\|\mathscr{P}_0\|+\frac{(\alpha_{\mathscr{U}}r+\beta_{\mathscr{U}})T^{\delta}}{\Gamma(\delta+1)}\le r,$$

and $\mathscr{U}$ is continuous, then the controlled model (2) *admits at least one solution $\mathscr{P}\in\mathscr{F}$.*

Proof. Fix $r>0$ as in the statement and set $B_r^*=\{\mathscr{P}\in\mathscr{F}:\|\mathscr{P}\|\le r\}$, a closed, bounded, convex subset of $\mathscr{F}$.

Step 1: $\mathscr{W}(B_r^*)\subset B_r^*$. For $\mathscr{P}\in B_r^*$ and $t\in[0,T]$,

$$|(\mathscr{W}\mathscr{P})(t)|\le\|\mathscr{P}_0\|+\frac{1}{\Gamma(\delta)}\int_0^t(t-\varpi)^{\delta-1}|\mathscr{U}(\varpi,\mathscr{P}(\varpi))|\,d\varpi.$$

By Assumption 1, $|\mathscr{U}(\varpi,\mathscr{P}(\varpi))|\le\alpha_{\mathscr{U}}\|\mathscr{P}\|+\beta_{\mathscr{U}}\le\alpha_{\mathscr{U}}r+\beta_{\mathscr{U}}$ for $\mathscr{P}\in B_r^*$, so

$$\sup_{t\in[0,T]}|(\mathscr{W}\mathscr{P})(t)|\le\|\mathscr{P}_0\|+(\alpha_{\mathscr{U}}r+\beta_{\mathscr{U}})\sup_{t\in[0,T]}\frac{1}{\Gamma(\delta)}\int_0^t(t-\varpi)^{\delta-1}\,d\varpi$$

$$= \|\mathscr{P}_0\| + \frac{(\alpha_{\mathscr{U}} r + \beta_{\mathscr{U}})T^{\delta}}{\Gamma(\delta+1)} \leq r,$$

using $\int_0^t (t-\varpi)^{\delta-1} d\varpi = t^{\delta}/\delta$ and $\Gamma(\delta+1) = \delta\Gamma(\delta)$. Hence $\mathscr{W}\mathscr{P} \in B_r^*$.

Step 2: Equicontinuity of $\mathscr{W}(B_r^*)$. For $\mathscr{P} \in B_r^*$ and $0 \leq z_1 < z_2 \leq T$,

$$\begin{aligned}|(\mathscr{W}\mathscr{P})(z_2) - (\mathscr{W}\mathscr{P})(z_1)| &\leq \frac{1}{\Gamma(\delta)}\Big| \int_0^{z_2} (z_2-\varpi)^{\delta-1}\mathscr{U}(\varpi, \mathscr{P}(\varpi))d\varpi \\ &\qquad - \int_0^{z_1} (z_1-\varpi)^{\delta-1}\mathscr{U}(\varpi, \mathscr{P}(\varpi))d\varpi\Big| \\ &\leq \frac{\alpha_{\mathscr{U}} r + \beta_{\mathscr{U}}}{\Gamma(\delta+1)}\left(z_2^{\delta} - z_1^{\delta}\right),\end{aligned}$$

which tends to 0 as $z_2 \to z_1$, uniformly over $\mathscr{P} \in B_r^*$, since $t \mapsto t^{\delta}$ is uniformly continuous on $[0,T]$. Hence $\mathscr{W}(B_r^*)$ is equicontinuous, and by Step 1 it is uniformly bounded; by the Arzelà–Ascoli theorem (Theorem 2.3) it is relatively compact in $\mathscr{F}$.

Step 3: Continuity of $\mathscr{W}$. Continuity of $\mathscr{U}$ in $\mathscr{P}$ (uniformly on compact time intervals) together with the dominated convergence theorem shows that $\mathscr{P}_n \to \mathscr{P}$ in $\mathscr{F}$ implies $\mathscr{W}\mathscr{P}_n \to \mathscr{W}\mathscr{P}$ in $\mathscr{F}$.

Combining Steps 1–3, $\mathscr{W} : B_r^* \to B_r^*$ is a continuous, compact self-map of a closed bounded convex set. By the Schauder fixed-point theorem (a special case of the Leray–Schauder alternative, Theorem 2.2, in which alternative (b) is excluded because $\mathscr{W}$ maps B_r^* into itself so that any $\lambda \in (0,1)$-scaled fixed point remains in the bounded set B_r^*), $\mathscr{W}$ has a fixed point $\mathscr{P} \in B_r^*$, which is the desired solution. □

4.2. Uniqueness of the solution.

Theorem 4.2 (Uniqueness)**.** *Under Assumption 2, if*

$$\frac{\hbar_{\mathscr{U}} T^{\delta}}{\Gamma(\delta+1)} < 1,$$

then the controlled model (2) *admits a unique solution in $\mathscr{F}$.*

Proof. For $\mathscr{P}_1, \mathscr{P}_2 \in \mathscr{F}$ and $t \in [0,T]$,

$$\begin{aligned}|(\mathscr{W}\mathscr{P}_1)(t) - (\mathscr{W}\mathscr{P}_2)(t)| &= \left|\frac{1}{\Gamma(\delta)}\int_0^t (t-\varpi)^{\delta-1}\big[\mathscr{U}(\varpi, \mathscr{P}_1(\varpi)) - \mathscr{U}(\varpi, \mathscr{P}_2(\varpi))\big]d\varpi\right| \\ &\leq \frac{1}{\Gamma(\delta)}\int_0^t (t-\varpi)^{\delta-1}\hbar_{\mathscr{U}}|\mathscr{P}_1(\varpi) - \mathscr{P}_2(\varpi)|\,d\varpi\end{aligned}$$

$$\leq \frac{\hbar_{\mathscr{U}}}{\Gamma(\delta)}\|\mathscr{P}_1-\mathscr{P}_2\|\int_0^t (t-\varpi)^{\delta-1}d\varpi$$
$$= \frac{\hbar_{\mathscr{U}} t^{\delta}}{\Gamma(\delta+1)}\|\mathscr{P}_1-\mathscr{P}_2\|$$
$$\leq \frac{\hbar_{\mathscr{U}} T^{\delta}}{\Gamma(\delta+1)}\|\mathscr{P}_1-\mathscr{P}_2\|.$$

Taking the supremum over $t \in [0,T]$ gives $\|\mathscr{W}\mathscr{P}_1 - \mathscr{W}\mathscr{P}_2\| \leq \kappa\|\mathscr{P}_1-\mathscr{P}_2\|$ with $\kappa = \hbar_{\mathscr{U}} T^{\delta}/\Gamma(\delta+1) < 1$ by hypothesis, so $\mathscr{W}$ is a contraction on the Banach space $\mathscr{F}$. By the Banach fixed-point theorem, $\mathscr{W}$ has a unique fixed point, i.e. the controlled model has a unique solution. □

Corollary 4.1. *Under the hypotheses of Theorem 4.2, the unique solution of* (2) *depends continuously on the initial data* $\mathscr{P}_0$ *and, for fixed admissible controls, is the limit of the Picard iteration* $\mathscr{P}_{n+1} = \mathscr{W}\mathscr{P}_n$, $\mathscr{P}_0(t) \equiv \mathscr{P}_0$, *with geometric convergence rate* $\kappa = \hbar_{\mathscr{U}} T^{\delta}/\Gamma(\delta+1)$.

4.3. Ulam–Hyers-type stability. Let $\Xi > 0$ and let $L_{\mathscr{U}} : [0,T) \to \mathbb{R}_+$ be continuous. Consider the inequalities

$$\left|{}^{C}D_t^{\delta} B(t) - \mathscr{U}(t, B(t))\right| \leq \Xi, \tag{4}$$

$$\left|{}^{C}D_t^{\delta} B(t) - \mathscr{U}(t, B(t))\right| \leq \Xi L_{\mathscr{U}}(t), \tag{5}$$

$$\left|{}^{C}D_t^{\delta} B(t) - \mathscr{U}(t, B(t))\right| \leq L_{\mathscr{U}}(t). \tag{6}$$

Definition 4.1. *The model is* Ulam–Hyers (UH) stable *if there exists* $J_{\mathscr{U}} > 0$ *such that for every* $\Xi > 0$ *and every* $B \in \mathscr{F}$ *satisfying* (4)*, there is a solution* $\mathscr{P} \in \mathscr{F}$ *of* (2) *with* $\sup_{t\in[0,T]} |B(t) - \mathscr{P}(t)| \leq \Xi J_{\mathscr{U}}$.

Definition 4.2. *The model is* generalized UH stable *if there exists* $K_{\mathscr{U}} \in C(\mathbb{R}_+, \mathbb{R}_+)$, $K_{\mathscr{U}}(0) = 0$*, such that for every* $B \in \mathscr{F}$ *satisfying* (4) *there is a solution* $\mathscr{P}$ *of* (2) *with* $|B(t) - \mathscr{P}(t)| \leq K_{\mathscr{U}}(\Xi)$.

Definition 4.3. *The model is* Ulam–Hyers–Rassias (UHR) stable *with respect to* $L_{\mathscr{U}}$ *if there exists* $U_{L_{\mathscr{U}}} > 0$ *such that for every* $\Xi > 0$ *and every* $B \in \mathscr{F}$ *satisfying* (5)*, there is a solution* $\mathscr{P}$ *of* (2) *with* $|B(t) - \mathscr{P}(t)| \leq L_{\mathscr{U}}(t)\, U_{L_{\mathscr{U}}}\, \Xi$.

Definition 4.4. *The model is* generalized UHR stable *with respect to $L_{\mathscr{U}}$ if there exists $U_{L_{\mathscr{U}}} > 0$ such that every $B \in \mathscr{F}$ satisfying* (6) *admits a solution $\mathscr{P}$ of* (2) *with $|B(t) - \mathscr{P}(t)| \leq L_{\mathscr{U}}(t)\, U_{L_{\mathscr{U}}}$.*

H 3. *There exists $\Upsilon_{L_{\mathscr{U}}} > 0$ such that $I_0^{\delta} L_{\mathscr{U}}(t) \leq \Upsilon_{L_{\mathscr{U}}} L_{\mathscr{U}}(t)$ for all $t \in [0,T)$.*

Lemma 4.1. *If $B \in \mathscr{F}$ satisfies* (4)*, then*

$$\sup_{t\in[0,T]} \left| B(t) - B_0 - \frac{1}{\Gamma(\delta)} \int_0^t (t-\varpi)^{\delta-1} \mathscr{U}(\varpi, B(\varpi))\, d\varpi \right| \leq \frac{\Xi T^{\delta}}{\Gamma(\delta+1)}.$$

Proof. Since B satisfies (4), there exists $\mathscr{L} \in \mathscr{F}$ with $|\mathscr{L}(t)| \leq \Xi$ such that ${}^{C}D_t^{\delta} B(t) = \mathscr{U}(t, B(t)) + \mathscr{L}(t)$, $B(0) = B_0$. Applying I^{δ} to both sides,

$$B(t) = B_0 + \frac{1}{\Gamma(\delta)} \int_0^t (t-\varpi)^{\delta-1} \mathscr{U}(\varpi, B(\varpi)) d\varpi + \frac{1}{\Gamma(\delta)} \int_0^t (t-\varpi)^{\delta-1} \mathscr{L}(\varpi) d\varpi,$$

so

$$\begin{aligned} \left| B(t) - B_0 - \frac{1}{\Gamma(\delta)} \int_0^t (t-\varpi)^{\delta-1} \mathscr{U}(\varpi, B(\varpi)) d\varpi \right| &\leq \frac{1}{\Gamma(\delta)} \int_0^t (t-\varpi)^{\delta-1} |\mathscr{L}(\varpi)| d\varpi \\ &\leq \frac{\Xi t^{\delta}}{\Gamma(\delta+1)} \leq \frac{\Xi T^{\delta}}{\Gamma(\delta+1)}. \end{aligned}$$

□

Theorem 4.3 (UH and generalized UH stability)**.** *Under Assumption 2, if $\hbar_{\mathscr{U}} T^{\delta}/\Gamma(\delta+1) < 1$, then the controlled model is UH stable and generalized UH stable, with*

$$J_{\mathscr{U}} = \frac{T^{\delta}/\Gamma(\delta+1)}{1 - \hbar_{\mathscr{U}} T^{\delta}/\Gamma(\delta+1)}.$$

Proof. Let $B \in \mathscr{F}$ satisfy (4) and let $\mathscr{P} \in \mathscr{F}$ be the (unique, by Theorem 4.2) solution of (2). Using the triangle inequality, Lemma 4.1, and Assumption 2,

$$\begin{aligned} \sup_{t\in[0,T]} |B(t) - \mathscr{P}(t)| &\leq \sup_{t\in[0,T]} \left| B(t) - B_0 - \frac{1}{\Gamma(\delta)} \int_0^t (t-\varpi)^{\delta-1} \mathscr{U}(\varpi, \mathscr{P}(\varpi)) d\varpi \right| \\ &\leq \sup_{t\in[0,T]} \left| B(t) - B_0 - \frac{1}{\Gamma(\delta)} \int_0^t (t-\varpi)^{\delta-1} \mathscr{U}(\varpi, B(\varpi)) d\varpi \right| \\ &\quad + \sup_{t\in[0,T]} \frac{1}{\Gamma(\delta)} \int_0^t (t-\varpi)^{\delta-1} |\mathscr{U}(\varpi, B(\varpi)) - \mathscr{U}(\varpi, \mathscr{P}(\varpi))|\, d\varpi \end{aligned}$$

$$\leq \frac{\Xi T^{\delta}}{\Gamma(\delta+1)} + \frac{\hbar_{\mathscr{U}} T^{\delta}}{\Gamma(\delta+1)} \sup_{t\in[0,T]} |B(t) - \mathscr{P}(t)|.$$

Rearranging (using $\hbar_{\mathscr{U}} T^{\delta}/\Gamma(\delta+1) < 1$) gives $\sup_{t\in[0,T]} |B(t) - \mathscr{P}(t)| \leq \Xi J_{\mathscr{U}}$, proving UH stability. Setting $K_{\mathscr{U}}(\Xi) = \Xi J_{\mathscr{U}}$, which satisfies $K_{\mathscr{U}}(0) = 0$, proves generalized UH stability. □

Theorem 4.4 (UHR and generalized UHR stability)**.** *Under Assumptions 2 and 3, the controlled model is UHR stable and generalized UHR stable with respect to $L_{\mathscr{U}}$, with*

$$U_{L_{\mathscr{U}}} = \Upsilon_{L_{\mathscr{U}}} E_{\beta}\left(\frac{\hbar_{\mathscr{U}}}{\Gamma(\delta)}\Gamma(\beta)T^{\beta}\right)$$

for a suitable auxiliary exponent $\beta > 0$.

Proof. The proof follows the same structure as Theorem 4.3, replacing the bound $\Xi T^{\delta}/\Gamma(\delta+1)$ of Lemma 4.1 by $\Xi\Upsilon_{L_{\mathscr{U}}} L_{\mathscr{U}}(t)$ (using Assumption 3), so that

$$|B(t) - \mathscr{P}(t)| \leq \Xi\Upsilon_{L_{\mathscr{U}}} L_{\mathscr{U}}(t) + \frac{\hbar_{\mathscr{U}}}{\Gamma(\delta)} \int_0^t (t-\varpi)^{\delta-1} |B(\varpi) - \mathscr{P}(\varpi)|\, d\varpi.$$

Applying the generalized Grönwall inequality (Theorem 2.4) to $x(t) = |B(t) - \mathscr{P}(t)|$ yields

$$|B(t) - \mathscr{P}(t)| \leq \Xi\Upsilon_{L_{\mathscr{U}}} L_{\mathscr{U}}(t) E_{\beta}\left(\frac{\hbar_{\mathscr{U}}}{\Gamma(\delta)}\Gamma(\beta)T^{\beta}\right),$$

which is the UHR estimate with $U_{L_{\mathscr{U}}}$ as stated. The generalized UHR case (inequality (6), with $\Xi = 1$ absorbed into $L_{\mathscr{U}}$) follows identically. □

These stability results guarantee that small perturbations of the model — arising, for instance, from measurement error in parameter estimation, from numerical discretization, or from model misspecification — produce correspondingly small, quantifiable deviations in the predicted state trajectory, which is an essential property for any model intended to inform clinical treatment decisions.

Remark 4.2 (Biological interpretation)**.** *Concretely, Theorem 4.3 says that if a candidate trajectory $B(t)$ — for instance, one obtained by fitting the model to a patient's longitudinal PSA measurements, or one computed with a slightly different numerical scheme or a perturbed parameter set — satisfies the governing equations only approximately, up to a uniform error Ξ, then $B(t)$ cannot drift arbitrarily far from a true solution $\mathscr{P}(t)$ of the exact model: the two*

remain within $\Xi J_{\mathscr{U}}$ of each other for all $t \in [0,T]$, with the explicit, computable constant $J_{\mathscr{U}}$ derived above. In practice this means that modest uncertainty in the estimated growth, killing, or mutation rates $e_1, e_2, a_1, a_2, m_1, \ldots$ (all of which enter $\hbar_{\mathscr{U}}$), or modest discretization error in the numerical scheme of Section 7, cannot produce a qualitatively different predicted disease trajectory — the model's predictions degrade gracefully, rather than catastrophically, under such perturbations. The UHR variant (Theorem 4.4) refines this further by allowing the error tolerance to vary with t through the weight $L_{\mathscr{U}}(t)$, which is useful when perturbations are expected to be time-dependent, e.g. larger early in treatment (when parameter estimates are least reliable) than at steady state.

5. Equilibria and Local Stability of the Uncontrolled Model

To complement the qualitative existence/uniqueness/stability results above, we briefly analyze the equilibria of the uncontrolled ($u_1 = u_2 = 0$) model, which correspond to the untreated (or treatment-holiday) dynamics and provide a baseline against which the effect of control can be measured.

5.1. Tumor-free equilibrium. Setting the right-hand side of (2) to zero with $u_1 = u_2 = 0$, the tumor-free equilibrium $E_0 = (0,0,Y^*,a_0,0)$ requires $X_1 = X_2 = 0$ and $\mathscr{J} = 0$ (since $\mathscr{J}$ has no source without immunotherapy, ${}^C D_t^\delta \mathscr{J} = -c\,\mathscr{J} = 0 \Rightarrow \mathscr{J} = 0$), $A = a_0$ (from $-\gamma(A-a_0) = 0$), and then, from ${}^C D_t^\delta Y = (W-\omega)Y + \varepsilon\,\mathscr{J}/(g_3+\mathscr{J}) = 0$ with $\mathscr{J} = 0$, either $Y^* = 0$ (if $W \neq \omega$) or Y^* arbitrary (if $W = \omega$); generically, for $W \neq \omega$, $E_0 = (0,0,0,a_0,0)$.

Proposition 3. *The tumor-free equilibrium $E_0 = (0,0,0,a_0,0)$ of the uncontrolled model is* never *locally asymptotically stable in the full five-dimensional sense: both the X_1- and X_2-direction Jacobian eigenvalues are unconditionally positive ($\lambda_1 = e_1 a_0 > 0$ and $\lambda_2 = e_2 > 0$, see the proof), independently of any other parameter value. Restricted to the invariant subspace $\{X_1 \equiv X_2 \equiv 0\}$ — i.e., considering only the $(Y,A,\mathscr{J})$-dynamics obtained by setting both tumor compartments identically to zero — E_0 is locally asymptotically stable in the Matignon sense (Theorem 2.5) if and only if $W < \omega$.*

Proof. We linearize (2) (with $u_1 = u_2 = 0$) about $E_0 = (0,0,0,a_0,0)$ and evaluate the full 5×5 Jacobian $J_{\mathscr{U}} = \partial \mathscr{U} / \partial \mathscr{P}$ using the general expressions of Appendix A (Section A.2), specialized to $X_1 = X_2 = \mathscr{J} = 0, A = a_0$.

Step 1: Evaluate each partial derivative at E_0. Since $X_1 = X_2 = 0$, the denominators $g_1 + X_1 + X_2 = g_1$ and $g_2 + X_1 + X_2 = g_2$ are simply the (strictly positive) half-saturation constants. Recall from Appendix A.2 that $\mathscr{U}_1 = X_1\, g(X_1, X_2, Y, A)$ with $g(0,0,0,a_0) = e_1 a_0 - (d_1 + m_1)(1 - 1) - 0 = e_1 a_0$; since $X_1 = 0$ at E_0, the product-rule terms $X_1\, \partial g / \partial(\cdot)$ vanish identically, leaving only the $g|_{E_0}$ contribution to $\partial \mathscr{U}_1 / \partial X_1$. Substituting $X_1 = X_2 = 0, A = a_0, Y = 0$ into the general formulas of Appendix A.2 term-by-term yields the exact values

$$\left.\frac{\partial \mathscr{U}_1}{\partial X_1}\right|_{E_0} = e_1 a_0, \qquad \left.\frac{\partial \mathscr{U}_1}{\partial X_2}\right|_{E_0} = 0, \qquad \left.\frac{\partial \mathscr{U}_1}{\partial Y}\right|_{E_0} = 0, \qquad \left.\frac{\partial \mathscr{U}_1}{\partial A}\right|_{E_0} = 0,$$

$$\left.\frac{\partial \mathscr{U}_2}{\partial X_1}\right|_{E_0} = m_1\left(1 - \frac{a_0}{a_0}\right) = 0, \qquad \left.\frac{\partial \mathscr{U}_2}{\partial X_2}\right|_{E_0} = e_2, \qquad \left.\frac{\partial \mathscr{U}_2}{\partial Y}\right|_{E_0} = 0, \qquad \left.\frac{\partial \mathscr{U}_2}{\partial A}\right|_{E_0} = 0,$$

$$\left.\frac{\partial \mathscr{U}_3}{\partial Y}\right|_{E_0} = W - \omega, \qquad \left.\frac{\partial \mathscr{U}_3}{\partial \mathscr{J}}\right|_{E_0} = \frac{\varepsilon g_3}{(g_3 + 0)^2} = \frac{\varepsilon}{g_3}, \qquad \left.\frac{\partial \mathscr{U}_4}{\partial A}\right|_{E_0} = -\gamma, \qquad \left.\frac{\partial \mathscr{U}_5}{\partial \mathscr{J}}\right|_{E_0} = -c,$$

with all remaining partial derivatives (e.g. $\partial \mathscr{U}_1 / \partial \mathscr{J}$, $\partial \mathscr{U}_4 / \partial X_1$, etc.) equal to zero, since $\mathscr{U}_1, \mathscr{U}_2$ do not depend on $\mathscr{J}$ and $\mathscr{U}_4, \mathscr{U}_5$ do not depend on X_1, X_2, Y.

Step 2: Write out the full Jacobian and identify its block structure. Ordering the state vector as $(X_1, X_2, Y, A, \mathscr{J})$, the Jacobian at E_0 is

$$J_{\mathscr{U}}(E_0) = \begin{pmatrix} e_1 a_0 & 0 & 0 & 0 & 0 \\ 0 & e_2 & 0 & 0 & 0 \\ 0 & 0 & W - \omega & 0 & \varepsilon / g_3 \\ 0 & 0 & 0 & -\gamma & 0 \\ 0 & 0 & 0 & 0 & -c \end{pmatrix}.$$

This matrix is lower-block-triangular (indeed, upper-triangular apart from the single off-diagonal entry ε / g_3 in the $(Y, \mathscr{J})$ position, which does not affect the diagonal), so its eigenvalues are exactly its five diagonal entries:

$$\lambda_1 = e_1 a_0, \quad \lambda_2 = e_2, \quad \lambda_3 = W - \omega, \quad \lambda_4 = -\gamma, \quad \lambda_5 = -c.$$

(This can be verified directly: expanding $\det(J_{\mathscr{U}}(E_0) - \lambda I)$ along the first, second, fourth, and fifth columns, each of which has only a single nonzero entry on the diagonal, successively reduces the determinant to a product of the diagonal entries minus λ, confirming the eigenvalues above; the off-diagonal entry ε/g_3 enters only the corresponding eigenvector, not the eigenvalue $\lambda_3 = W - \omega$, since column 3 of $J_{\mathscr{U}}(E_0) - \lambda I$ has its only nonzero entries on the diagonal.)

Step 3: Apply the Matignon criterion (Theorem 2.5) to each eigenvalue. All five eigenvalues are real, so $|\arg(\lambda_i)| \in \{0, \pi\}$: $|\arg(\lambda_i)| = 0 < \delta\pi/2$ (unstable direction) if $\lambda_i > 0$, and $|\arg(\lambda_i)| = \pi > \delta\pi/2$ (stable direction, since $\delta\pi/2 < \pi/2 < \pi$ for $\delta \in (0,1)$) if $\lambda_i < 0$. Hence:

- $\lambda_4 = -\gamma < 0$ and $\lambda_5 = -c < 0$ (since $\gamma, c > 0$ by definition): these two directions are always locally stable, independently of any other parameter.
- $\lambda_1 = e_1 a_0 > 0$ *unconditionally* (since $e_1, a_0 > 0$ by definition): the X_1-direction is *never* locally stable at E_0, for any parameter values.
- $\lambda_2 = e_2 > 0$ *unconditionally* (since $e_2 > 0$ by definition): the X_2-direction is likewise *never* locally stable at E_0, for any parameter values.
- $\lambda_3 = W - \omega$ is stable if and only if $W < \omega$.

E_0 is locally asymptotically stable, in the sense of Theorem 2.5, if and only if *all five* eigenvalues satisfy the Matignon condition; since $\lambda_1 = e_1 a_0 > 0$ and $\lambda_2 = e_2 > 0$ can never satisfy it, E_0 is, strictly speaking, never locally asymptotically stable in the full five-dimensional sense. The statement of the proposition should therefore be read, as is standard practice for equilibria that are unconditionally unstable in some biologically distinguished directions, as characterizing stability of the remaining three directions (equivalently, stability of E_0 restricted to the invariant subspace $X_1 \equiv X_2 \equiv 0$, on which neither tumor-direction plays a role): on this subspace, E_0 is locally asymptotically stable if and only if $W < \omega$, which is the content of the proposition. This is itself biologically meaningful, and considerably sharper than a conditional statement would be: it formalizes the fact that *any* small tumor population — whether AD or AI, however small — is never locally damped by the untreated dynamics near E_0; the untreated system offers no intrinsic barrier to the initial establishment of either phenotype, which is precisely the mathematical content of describing PC as a disease requiring active intervention rather than one that might resolve spontaneously. □

Remark 5.1. *Proposition 3 shows that, at* any *biologically admissible parameter values ($e_1, a_0 > 0$ and $e_2 > 0$ always), a small untreated tumor of either phenotype is predicted to grow near E_0 — consistent with the untreated trajectories in Figure 1(a)–(b), which show both X_1 and X_2 rising from their (small, relative to Q) initial values. This underscores the clinical necessity of active androgen suppression and/or immunotherapy (captured by the controls u_1, u_2) to prevent tumor establishment; the unconditional instability of both tumor directions removes the need to verify any parameter inequality and holds for the entire biologically meaningful parameter range.*

5.2. Coexistence / treated equilibria. Under sustained control ($u_1(t) \equiv \bar{u}_1 > 0$ constant, corresponding to CAD), the androgen level relaxes to $\bar{A} = a_0(1-\bar{u}_1)$, and setting the remaining right-hand sides to zero yields a coexistence equilibrium $E^* = (X_1^*, X_2^*, Y^*, \bar{A}, \mathscr{J}^*)$ solving the coupled algebraic system

$$e_1\bar{A}\left(1-\tfrac{X_1^*+\alpha X_2^*}{Q}\right)-(d_1+m_1)\left(1-\tfrac{\bar{A}}{a_0}\right)-\tfrac{a_1 Y^* X_1^*}{g_1+X_1^*+X_2^*}=0,$$

together with analogous equations for $X_2^*, Y^*, \mathscr{J}^*$; because of the nonlinear, rational dependence on X_1^*, X_2^*, this system does not admit a closed-form solution in general, and E^* is instead located numerically for each parameter set (see Section 8). Local stability of E^* is assessed via the Matignon criterion applied to the (numerically evaluated) Jacobian of $\mathscr{U}$ at E^*; this analysis is summarized in Appendix A.

6. Optimal Control Problem

6.1. Cost functional. We seek admissible controls $(u_1, u_2) \in \mathscr{U}_{ad}$, where

$$\mathscr{U}_{ad} = \left\{(u_1,u_2) \text{ measurable} : 0 \le u_1(t) \le u_1^{\max},\ 0 \le u_2(t) \le u_2^{\max},\ t \in [0,T]\right\},$$

that minimize the cost functional

$$J(u_1,u_2) = \int_0^T \left[w_1 X_1(t) + w_2 X_2(t) + \frac{1}{2}w_3 u_1^2(t) + \frac{1}{2}w_4 u_2^2(t)\right] dt, \tag{7}$$

subject to the state system (2). Here $w_1, w_2 > 0$ weight the AD and AI tumor burden, and $w_3, w_4 > 0$ penalize the cost/toxicity of ADT and immunotherapy, respectively; the quadratic control terms reflect the standard assumption of diminishing returns and increasing marginal

cost of treatment intensity, widely used in optimal control formulations of chemotherapy and immunotherapy scheduling.

6.2. Existence of an optimal control.

Proposition 4 (Existence of optimal control)**.** *There exists an optimal control pair* $(u_1^*, u_2^*) \in \mathscr{U}_{ad}$ *minimizing J subject to* (2)*.*

We verify existence via a fractional-order adaptation of the classical Filippov–Cesari existence theorem for optimal controls, whose hypotheses are: (F1) the admissible control set is nonempty, closed, bounded, and convex; (F2) the state trajectories corresponding to admissible controls are uniformly bounded and equicontinuous on $[0,T]$; (F3) the velocity set $\{(\mathscr{U}(t,\mathscr{P},u_1,u_2), w_1X_1 + w_2X_2 + \frac{1}{2}w_3u_1^2 + \frac{1}{2}w_4u_2^2) : (u_1,u_2) \in \mathscr{U}_{ad}\} \subset \mathbb{R}^6$ is convex for each fixed $(t,\mathscr{P})$; and (F4) the cost integrand is bounded below. We verify each in turn.

Proof. Verification of (F1). $\mathscr{U}_{ad} = [0,u_1^{\max}] \times [0,u_2^{\max}]$-valued measurable functions on $[0,T]$ form a nonempty (it contains, e.g., $u_1 \equiv u_2 \equiv 0$), closed, and bounded subset of $L^2([0,T])^2$, and is convex because for $(u_1,u_2),(v_1,v_2) \in \mathscr{U}_{ad}$ and $\theta \in [0,1]$, the pointwise convex combination $\theta(u_1,u_2) + (1-\theta)(v_1,v_2)$ again takes values in $[0,u_1^{\max}] \times [0,u_2^{\max}]$ at every t (since this box is itself convex), and is measurable as a pointwise combination of measurable functions.

Verification of (F2). By Proposition 2, for *every* admissible control pair the corresponding state trajectory satisfies $A(t) \le \max(A_0,a_0)$ for all t, and $X_1(t) + X_2(t)$ is bounded above by a constant M_1 depending only on Q,α,β and the initial data — crucially, *not* on the particular control chosen, since the argument in Proposition 2 used only that $u_1(t) \in [0,1]$, a property shared by every element of $\mathscr{U}_{ad}$. Given this uniform bound on X_1, X_2, A, the right-hand sides of the Y- and $\mathscr{J}$-equations, $(W-\omega)Y + \varepsilon\mathscr{J}/(g_3+\mathscr{J})$ and $-c\mathscr{J} + u_2(t)$, are themselves bounded by an affine function of $(Y,\mathscr{J})$ with control-independent coefficients (using $u_2(t) \le u_2^{\max}$), so a further application of the same fractional comparison argument used in Proposition 2 yields a control-independent bound $Y(t) + \mathscr{J}(t) \le M_2$ for all $t \in [0,T]$ and all admissible controls. Hence there is a single compact set $K \subset \mathbb{R}^5_{\ge 0}$, namely $K = \{\mathscr{P} \ge 0 : X_1 + X_2 \le M_1,\ A \le \max(A_0,a_0),\ Y + \mathscr{J} \le M_2\}$, containing $\mathscr{P}(t)$ for every $t \in [0,T]$ and every admissible control. Equicontinuity of the family $\{\mathscr{P}(\cdot;u_1,u_2) : (u_1,u_2) \in \mathscr{U}_{ad}\}$ then follows exactly as in Step 2

of the proof of Theorem 4.1 (the argument there did not use any property specific to a fixed control, only the sub-linear growth bound of Assumption 1, which holds uniformly over $\mathscr{U}_{ad}$ on the compact set K since $\mathscr{U}$ is continuous and $K \times [0, u_1^{\max}] \times [0, u_2^{\max}]$ is compact).

Verification of (F3). Fix $(t, \mathscr{P})$. Since $\mathscr{U}_4$ is affine in u_1 and $\mathscr{U}_5$ is affine in u_2 (and $\mathscr{U}_1, \mathscr{U}_2, \mathscr{U}_3$ do not depend on u_1, u_2 at all), the map $(u_1, u_2) \mapsto \mathscr{U}(t, \mathscr{P}, u_1, u_2)$ is affine, hence its image over the convex set $\mathscr{U}_{ad}(t) = [0, u_1^{\max}] \times [0, u_2^{\max}]$ is again convex (a line segment's image under an affine map is a line segment). The cost integrand $w_1 X_1 + w_2 X_2 + \frac{1}{2} w_3 u_1^2 + \frac{1}{2} w_4 u_2^2$ is a convex function of (u_1, u_2) for fixed $\mathscr{P}$ (sum of a constant, in u, term and a positive-definite quadratic form, since $w_3, w_4 > 0$). The velocity set in (F3) is therefore the image of the convex set $\mathscr{U}_{ad}(t)$ under the map $(u_1, u_2) \mapsto (\mathscr{U}(t, \mathscr{P}, u_1, u_2), c(t, \mathscr{P}, u_1, u_2))$ where c denotes the cost integrand; because the $\mathscr{U}$-component is affine and the c-component is convex in (u_1, u_2), the "epigraph-type" set $\{(\mathscr{U}(t, \mathscr{P}, u_1, u_2), z) : (u_1, u_2) \in \mathscr{U}_{ad}(t),\ z \geq c(t, \mathscr{P}, u_1, u_2)\}$ is convex, which is precisely the form of convexity required by the Filippov–Cesari theorem to guarantee that a minimizing sequence of controls can be replaced by an actual (not merely relaxed) admissible control in the limit.

Verification of (F4). The cost integrand is a sum of nonnegative terms ($X_1, X_2 \geq 0$ by Proposition 1, and $u_1^2, u_2^2 \geq 0$), hence bounded below by 0.

Conclusion. With (F1)–(F4) verified, the fractional-order Filippov–Cesari argument proceeds exactly as in the classical (integer-order) case: let $(u_1^{(n)}, u_2^{(n)})$ be a minimizing sequence for J over $\mathscr{U}_{ad}$, with corresponding state trajectories $\mathscr{P}^{(n)}$. By (F2) and the Arzelà–Ascoli theorem (Theorem 2.3), a subsequence (not relabeled) of $\mathscr{P}^{(n)}$ converges uniformly on $[0, T]$ to some $\mathscr{P}^* \in C([0, T], \mathbb{R}^5)$; by weak compactness of bounded sets in $L^2([0, T])^2$ (using (F1)), a further subsequence of $(u_1^{(n)}, u_2^{(n)})$ converges weakly to some $(u_1^*, u_2^*) \in \mathscr{U}_{ad}$ (weak limits of $[0, u_i^{\max}]$-valued functions remain $[0, u_i^{\max}]$-valued a.e., by convexity and closedness of the box). The convexity established in (F3) guarantees, via the fractional-order analogue of the standard weak-lower-semicontinuity argument for the integral functional J combined with passage to the limit in the (weakly continuous, since affine and bounded) integral fixed-point representation (2) of the state equation, that $\mathscr{P}^*$ is the state trajectory corresponding to (u_1^*, u_2^*), and that

$$J(u_1^*, u_2^*) \leq \liminf_{n \to \infty} J(u_1^{(n)}, u_2^{(n)}) = \inf_{(u_1, u_2) \in \mathscr{U}_{ad}} J(u_1, u_2).$$

Since $(u_1^*, u_2^*) \in \mathscr{U}_{ad}$, this infimum is attained, i.e. (u_1^*, u_2^*) is an optimal control pair. □

6.3. Necessary optimality conditions. To characterize the optimal control, we introduce the fractional-order Hamiltonian

$$\mathscr{H}(t, \mathscr{P}, u_1, u_2, \lambda) = w_1 X_1 + w_2 X_2 + \tfrac{1}{2} w_3 u_1^2 + \tfrac{1}{2} w_4 u_2^2 + \sum_{i=1}^{5} \lambda_i \mathscr{U}_i(t, \mathscr{P}, u_1, u_2),$$

where $\lambda_1, \ldots, \lambda_5$ are the co-state variables associated with $X_1, X_2, Y, A, \mathscr{J}$, respectively.

Theorem 6.1 (Fractional-order Pontryagin Maximum Principle)**.** *Let (u_1^*, u_2^*) be an optimal control pair for problem* (7)–(2) *with corresponding optimal state trajectory $\mathscr{P}^*$. Then there exists a co-state vector $\lambda = (\lambda_1, \ldots, \lambda_5)$ such that:*

*(i) (*State equations*)* ${}^{C}D_t^{\delta} \mathscr{P}^* = \partial \mathscr{H} / \partial \lambda = \mathscr{U}(t, \mathscr{P}^*, u_1^*, u_2^*)$*, with* $\mathscr{P}^*(0) = \mathscr{P}_0$*;*

*(ii) (*Co-state equations*)*

$$ {}_{t}^{C}D_T^{\delta} \lambda_i = -\frac{\partial \mathscr{H}}{\partial \mathscr{P}_i}\Big|_{(\mathscr{P}^*, u_1^*, u_2^*, \lambda)}, \qquad \lambda_i(T) = 0, \quad i = 1, \ldots, 5,$$

where ${}_{t}^{C}D_T^{\delta}$ denotes the right Caputo fractional derivative on $[0, T]$;

*(iii) (*Optimality condition*) for a.e. $t \in [0, T]$,*

$$\mathscr{H}(t, \mathscr{P}^*(t), u_1^*(t), u_2^*(t), \lambda(t)) \leq \mathscr{H}(t, \mathscr{P}^*(t), u_1, u_2, \lambda(t))$$

for all $(u_1, u_2) \in [0, u_1^{\max}] \times [0, u_2^{\max}]$.

Proof. This is the fractional-order analogue of the classical Pontryagin Maximum Principle; we give the complete derivation, following the fractional calculus-of-variations approach of Agrawal, adapted to the present control-constrained, vector-valued setting.

Step 1: Needle variation and the variational (linearized) state equation. Fix a Lebesgue point $\tau \in (0, T)$ of $t \mapsto \mathscr{U}(t, \mathscr{P}^*(t), u_1^*(t), u_2^*(t))$, an arbitrary admissible value $(v_1, v_2) \in [0, u_1^{\max}] \times [0, u_2^{\max}]$, and $\varepsilon > 0$ small. Define the needle-perturbed control

$$u_{i,\varepsilon}(t) = \begin{cases} v_i, & t \in [\tau, \tau + \varepsilon], \\ u_i^*(t), & \text{otherwise}, \end{cases} \qquad i = 1, 2,$$

and let $\mathscr{P}_\varepsilon$ denote the corresponding state trajectory, i.e. the solution of (2) with $\mathscr{U}(\cdot, \cdot, u_{1,\varepsilon}, u_{2,\varepsilon})$ in place of $\mathscr{U}(\cdot, \cdot, u_1^*, u_2^*)$. Write $\delta \mathscr{P}(t) = \lim_{\varepsilon \to 0^+} \varepsilon^{-1} \big(\mathscr{P}_\varepsilon(t) - \mathscr{P}^*(t) \big)$ for

the (first-order) state variation, which exists by the continuous dependence on parameters guaranteed by Theorem 4.2. Subtracting the integral equation (2) for $\mathscr{P}_\varepsilon$ from that for $\mathscr{P}^*$, dividing by ε, and letting $\varepsilon \to 0^+$, one obtains (using that the needle interval $[\tau, \tau+\varepsilon]$ shrinks to the point τ, contributing a jump of size $\Delta\mathscr{U}(\tau) := \mathscr{U}(\tau, \mathscr{P}^*(\tau), v_1, v_2) - \mathscr{U}(\tau, \mathscr{P}^*(\tau), u_1^*(\tau), u_2^*(\tau))$ to the integrand at $t = \tau$, and that elsewhere the perturbation propagates through the Jacobian $D_{\mathscr{P}}\mathscr{U}(t, \mathscr{P}^*(t), u_1^*(t), u_2^*(t))$) the *fractional variational equation*

$$(8)\quad {}^{C}D_t^{\delta}\,\delta\mathscr{P}(t) = D_{\mathscr{P}}\mathscr{U}\left(t, \mathscr{P}^*(t), u_1^*(t), u_2^*(t)\right)\delta\mathscr{P}(t) + \Delta\mathscr{U}(\tau)\,\delta(t-\tau), \qquad \delta\mathscr{P}(0) = 0,$$

where $\delta(t-\tau)$ denotes the Dirac mass at τ and $D_{\mathscr{P}}\mathscr{U}$ is the 5×5 Jacobian of $\mathscr{U}$ with respect to $\mathscr{P}$ (given explicitly in Appendix A.2). Equivalently, in mild (fixed-point) form,

$$(9)\quad \delta\mathscr{P}(t) = \frac{1}{\Gamma(\delta)}\int_0^t (t-s)^{\delta-1} D_{\mathscr{P}}\mathscr{U}(s, \mathscr{P}^*(s), u_1^*(s), u_2^*(s))\,\delta\mathscr{P}(s)\,ds + \frac{(t-\tau)_+^{\delta-1}}{\Gamma(\delta)}\Delta\mathscr{U}(\tau), \qquad t \geq \tau.$$

Step 2: First-order variation of the cost functional. Since

$$J(u_1,u_2) = \int_0^T \mathscr{L}(\mathscr{P}(t), u_1(t), u_2(t))\,dt, \qquad \mathscr{L} = w_1X_1 + w_2X_2 + \tfrac{1}{2}w_3u_1^2 + \tfrac{1}{2}w_4u_2^2,$$

a first-order expansion in ε gives

$$(10)\quad \begin{aligned}\delta J &:= \lim_{\varepsilon\to 0^+}\frac{J(u_{1,\varepsilon}, u_{2,\varepsilon}) - J(u_1^*, u_2^*)}{\varepsilon}\\ &= \int_0^T \nabla_{\mathscr{P}}\mathscr{L}(\mathscr{P}^*(t), u_1^*(t), u_2^*(t))\cdot\delta\mathscr{P}(t)\,dt\\ &\quad + \nabla_u\mathscr{L}(\mathscr{P}^*(\tau), u_1^*(\tau), u_2^*(\tau))\cdot(v - u^*(\tau)),\end{aligned}$$

where the second (boundary) term arises from the needle's direct effect on the integrand over $[\tau, \tau+\varepsilon]$, of length ε, and $\nabla_{\mathscr{P}}\mathscr{L} = (w_1, w_2, 0, 0, 0)$.

Step 3: The adjoint (co-state) system and fractional integration by parts. To evaluate the integral term in (10) without needing $\delta\mathscr{P}$ explicitly, introduce the co-state $\lambda : [0,T] \to \mathbb{R}^5$ as the solution of the *adjoint* fractional system

$$(11)\quad {}_{t}^{C}D_T^{\delta}\lambda(t) = -D_{\mathscr{P}}\mathscr{U}(t, \mathscr{P}^*(t), u_1^*(t), u_2^*(t))^{\top}\lambda(t) - \nabla_{\mathscr{P}}\mathscr{L}(\mathscr{P}^*(t), u_1^*(t), u_2^*(t)), \qquad \lambda(T) = 0,$$

where ${}_t^C D_T^\delta$ is the right Caputo derivative on $[0,T]$. This choice is precisely dictated by the fractional integration-by-parts identity of Appendix A (Section A.1):

$$\int_0^T \lambda(t)\cdot {}^C D_t^\delta \delta\mathscr{P}(t)\,dt = \int_0^T \delta\mathscr{P}(t)\cdot {}_t^C D_T^\delta \lambda(t)\,dt,$$

which holds because $\delta\mathscr{P}(0)=0$ and $\lambda(T)=0$ eliminate the boundary terms of the identity. Substituting the variational equation (8) for ${}^C D_t^\delta \delta\mathscr{P}$ on the left-hand side and the adjoint equation (11) for ${}_t^C D_T^\delta \lambda$ on the right-hand side, and using the sifting property of the Dirac mass to evaluate the term involving $\delta(t-\tau)$, gives

$$\int_0^T \lambda(t)\cdot\Big[D_{\mathscr{P}}\mathscr{U}\,\delta\mathscr{P}(t)\Big]dt + \lambda(\tau)\cdot\Delta\mathscr{U}(\tau) = -\int_0^T \delta\mathscr{P}(t)\cdot\Big[D_{\mathscr{P}}\mathscr{U}^\top\lambda(t) + \nabla_{\mathscr{P}}\mathscr{L}\Big]dt,$$

and since $\lambda(t)\cdot[D_{\mathscr{P}}\mathscr{U}\,\delta\mathscr{P}(t)] = \delta\mathscr{P}(t)\cdot[D_{\mathscr{P}}\mathscr{U}^\top\lambda(t)]$ (transpose identity for the bilinear form), the corresponding terms cancel on both sides, leaving the key identity

$$\int_0^T \nabla_{\mathscr{P}}\mathscr{L}(\mathscr{P}^*(t),u_1^*(t),u_2^*(t))\cdot\delta\mathscr{P}(t)\,dt = \lambda(\tau)\cdot\Delta\mathscr{U}(\tau). \tag{12}$$

Step 4: Substituting into δJ and deriving the optimality condition. Substituting (12) into (10) gives

$$\delta J = \lambda(\tau)\cdot\Delta\mathscr{U}(\tau) + \nabla_u\mathscr{L}(\mathscr{P}^*(\tau),u_1^*(\tau),u_2^*(\tau))\cdot(v-u^*(\tau)).$$

Recalling that $\Delta\mathscr{U}(\tau) = \mathscr{U}(\tau,\mathscr{P}^*(\tau),v_1,v_2) - \mathscr{U}(\tau,\mathscr{P}^*(\tau),u_1^*(\tau),u_2^*(\tau))$ and that the fractional-order Hamiltonian is defined as $\mathscr{H}(t,\mathscr{P},u_1,u_2,\lambda) = \mathscr{L}(\mathscr{P},u_1,u_2) + \lambda\cdot\mathscr{U}(t,\mathscr{P},u_1,u_2)$, this expression is exactly

$$\delta J = \mathscr{H}(\tau,\mathscr{P}^*(\tau),v_1,v_2,\lambda(\tau)) - \mathscr{H}(\tau,\mathscr{P}^*(\tau),u_1^*(\tau),u_2^*(\tau),\lambda(\tau)).$$

Since (u_1^*,u_2^*) is optimal, $J(u_{1,\varepsilon},u_{2,\varepsilon}) \geq J(u_1^*,u_2^*)$ for every admissible needle perturbation and every sufficiently small $\varepsilon>0$, so $\delta J \geq 0$ for every admissible (v_1,v_2), i.e.

$$\mathscr{H}(\tau,\mathscr{P}^*(\tau),u_1^*(\tau),u_2^*(\tau),\lambda(\tau)) \leq \mathscr{H}(\tau,\mathscr{P}^*(\tau),v_1,v_2,\lambda(\tau))$$

for all $(v_1,v_2)\in[0,u_1^{\max}]\times[0,u_2^{\max}]$. Since τ was an arbitrary Lebesgue point (hence a.e. point of $[0,T]$), this establishes optimality condition (iii). Equation (11) is exactly condition (ii), since $-\partial\mathscr{H}/\partial\mathscr{P}_i = -\nabla_{\mathscr{P}}\mathscr{L}_i - (D_{\mathscr{P}}\mathscr{U}^\top\lambda)_i$ componentwise (using $\partial(\lambda\cdot\mathscr{U})/\partial\mathscr{P}_i = (D_{\mathscr{P}}\mathscr{U}^\top\lambda)_i$), and condition (i) is simply the state equation (2) evaluated along the optimal trajectory, which holds by definition of $\mathscr{P}^*$. This completes the derivation of all three conditions. □

Corollary 6.1 (Explicit optimal control characterization)**.** *Since $\mathscr{H}$ is quadratic and strictly convex in (u_1,u_2), condition (iii) of Theorem 6.1 is equivalent to the pointwise stationarity conditions $\partial\mathscr{H}/\partial u_1 = 0$, $\partial\mathscr{H}/\partial u_2 = 0$, projected onto the admissible box, giving*

$$
\begin{aligned}
u_1^*(t) &= \min\left\{u_1^{\max},\ \max\left\{0,\ \frac{\gamma a_0 \lambda_4(t)}{w_3}\right\}\right\},\\
u_2^*(t) &= \min\left\{u_2^{\max},\ \max\left\{0,\ -\frac{\lambda_5(t)}{w_4}\right\}\right\}.
\end{aligned}
\tag{13}
$$

Proof. Differentiating $\mathscr{H}$ with respect to u_1: $\partial\mathscr{H}/\partial u_1 = w_3u_1 + \lambda_4\,\partial\mathscr{U}_4/\partial u_1 = w_3u_1 - \gamma a_0\lambda_4$ (since $\mathscr{U}_4 = -\gamma(A - a_0(1-u_1))$ so $\partial\mathscr{U}_4/\partial u_1 = -\gamma a_0$, giving $w_3u_1 - \gamma a_0\lambda_4 = 0 \Rightarrow u_1 = \gamma a_0\lambda_4/w_3$). Similarly, $\partial\mathscr{H}/\partial u_2 = w_4u_2 + \lambda_5\,\partial\mathscr{U}_5/\partial u_2 = w_4u_2 + \lambda_5$ (since $\mathscr{U}_5 = -c\,\mathscr{J} + u_2$), giving the unconstrained stationary point $u_2 = -\lambda_5/w_4$. Because $\mathscr{H}$ is strictly convex (quadratic with positive coefficients w_3, w_4) in each control separately, these stationary points are minimizers of $\mathscr{H}$ over $\mathbb{R}$; projecting onto $[0,u_1^{\max}]$ and $[0,u_2^{\max}]$ respectively (since $\mathscr{H}$ is convex, the constrained minimizer is the projection of the unconstrained minimizer onto the box) gives (13). □

Equation (13) shows that the optimal ADT intensity is proportional to the co-state λ_4 associated with androgen suppression, while the optimal immunotherapy dosage is proportional to the (negative) co-state λ_5 associated with the dendritic-cell compartment, each clipped to the admissible control range — the fractional-order analogue of the classical bang–bang/interior characterization familiar from integer-order optimal control of tumor–immune systems.

7. Numerical Scheme

7.1. Fractional Euler / product-integration method. The forward state system (2) and the backward co-state system of Theorem 6.1 are solved iteratively using a **forward–backward sweep method**, in which each sweep uses a fractional Euler (product-integration) scheme for the corresponding fractional initial-value problem. For a generic scalar Caputo initial value problem ${}^{C}D_t^{\delta}x(t) = f(t,x(t))$, $x(0) = x_0$, on a grid $t_n^* = nh$, $n = 0,\dots,N$, the scheme reads

$$
x(t_{n+1}^*) = x_0 + \frac{h^{\delta}}{\Gamma(\delta+1)}\sum_{j=0}^{n}\Big[(n-j+1)^{\delta} - (n-j)^{\delta}\Big]f(t_j^*,x(t_j^*)),
\tag{14}
$$

obtained by approximating f by a piecewise-constant interpolant on each subinterval $[t_j^*, t_{j+1}^*]$ and evaluating the resulting sum of incomplete Beta-type integrals exactly; this is the discretized form of the fixed-point equation (2) and, unlike a naive single-term Euler update, correctly incorporates the memory kernel $(t-\varpi)^{\delta-1}$ of the Caputo derivative through the weights $(n-j+1)^{\delta}-(n-j)^{\delta}$. (When these weights are replaced by the single most-recent term, i.e. one restricts the sum in (14) to $j=n$ only, one recovers the simplified one-step recursion used for illustrative purposes in [25]; we use the full memory sum (14) throughout our numerical experiments for accuracy.) Applied componentwise to the vector system (2), with the control values $u_1(t_j^*), u_2(t_j^*)$ substituted at each grid point, this yields the forward update used in the algorithm below. A structurally identical scheme, applied on the reversed grid $\tau_k = T - t_{N-k}^*$ using the right Caputo derivative, is used for the co-state system.

7.2. Forward–backward sweep algorithm.

1. Initialize a guess for (u_1, u_2) over the grid $\{t_p^*\}_{p=0}^N$.
2. Solve the state system (2) forward in time using (14).
3. Solve the co-state system of Theorem 6.1 backward in time using the corresponding right-Caputo analogue of (14), starting from $\lambda(T)=0$.
4. Update the control estimate at each grid point using (13), taking a convex combination $u^{(k+1)} = \theta\, u^{(k)} + (1-\theta)\, u^{*,(k+1)}$, $\theta \in (0,1)$, of the previous and newly computed control to promote convergence of the sweep.
5. Repeat steps 2–4 until the relative change in (u_1, u_2), $\mathscr{P}$, and λ between successive iterations falls below a prescribed tolerance tol.

7.3. Convergence and stability analysis. We first derive the local truncation error for the simplified, single-term update obtained by retaining only the most recent ($j=n$) term of the memory sum in (14) — i.e. the scheme

$$X_1^{\text{num,simplified}}(t_{p+1}^*) = X_1(t_p^*) + \mathscr{U}_1(t_p^*, X_1(t_p^*))\,\frac{h^{\delta}}{\Gamma(\delta+1)},$$

which is the update used for exposition in [25] — and then relate this bound to the full-memory scheme (14) that is actually implemented and used throughout our numerical experiments (Remark 7.1 below).

Expanding the exact solution $X_1(t)$ using the generalized (fractional) Taylor formula about $t = t_p^*$,

$$X_1(t_{p+1}^*) = X_1(t_p^*) + {}^C D_t^{\delta} X_1(t_p^*)\, h^{\delta} + \tfrac{1}{2}\, {}^C D_t^{2\delta} X_1(t_p^*)\, h^{2\delta} + O(h^{3\delta}), \tag{15}$$

and comparing with $X_1^{\text{num,simplified}}$ above shows that the local truncation error of the simplified update at each step is

$$E_{\text{loc}}(t_{p+1}^*) = X_1(t_{p+1}^*) - X_1^{\text{num,simplified}}(t_{p+1}^*) = O(h^{2\delta}),$$

so that, over $N = T/h$ steps, the global error accumulates to

$$E_{\text{glob}}(T) = O(N \cdot h^{2\delta}) = O(h^{2\delta-1}) \cdot T = O(h^{\delta})$$

(using $N = T/h$), confirming first-order (in the fractional sense) convergence of the simplified scheme as $h \to 0$.

Remark 7.1 (Relation to the full-memory scheme actually used)**.** *The full-memory update* (14) *used throughout Sections 8–8.4 is the exact evaluation, via the incomplete-Beta-type weights* $(n-j+1)^{\delta} - (n-j)^{\delta}$*, of the fractional integral of the piecewise-constant interpolant of* $\mathscr{U}$ *over* all *past subintervals* $[t_j^*, t_{j+1}^*]$*,* $j = 0, \ldots, n$*; this is precisely the classical fractional (product-integration) Euler / one-step Adams–Bashforth method analyzed by Diethelm, Ford, and Freed* [42]*, who establish a global convergence order of* $O(h)$ *(and, more precisely,* $O(h^{\min(2,1+\delta)})$ *for the associated predictor-corrector variant) for exactly this quadrature rule. The simplified single-term update analyzed above is a further truncation of the same memory sum to its most recent term only, discarding the (positive, since* $\mathscr{U}$ *need not have constant sign but the weights themselves are positive and summable) contribution of all earlier subintervals; it is therefore a* less *accurate approximation of the same underlying integral than* (14)*, and cannot have smaller local truncation error at any fixed step. Consequently, the* $O(h^{\delta})$ *global convergence order derived above for the simplified update is a valid (and, in light of* [42]*, conservative) upper bound on the global error of the full-memory scheme* (14) *actually implemented and used for all simulations in this paper; the numerical step-halving check reported in the remark below, which is performed on the full-memory scheme itself, directly confirms this order empirically rather than relying on the bound by extrapolation alone.*

For local stability, consider a small perturbation $\Delta X_1(t_p^*)$. Linearizing the update (14) (restricted to its leading, $j = n$ term, for a local stability heuristic) gives

$$\Delta X_1(t_{p+1}^*) = \Delta X_1(t_p^*) \left[1 + \frac{\partial \mathscr{U}_1}{\partial X_1}(t_p^*, X_1(t_p^*)) \, \frac{h^\delta}{\Gamma(\delta+1)} \right],$$

so that perturbations do not grow (i.e. the amplification factor above has magnitude at most 1) provided

$$h \le \left[\Gamma(\delta+1) \Big/ \left| \frac{\partial \mathscr{U}_1}{\partial X_1} \right| \right]^{1/\delta}, \tag{16}$$

which is the step-size stability bound used to select h in the simulations of Section 8; analogous bounds hold componentwise for $X_2, Y, A, \mathscr{J}$ (and for the co-state components, using the corresponding partial derivatives of $-\partial \mathscr{H} / \partial \mathscr{P}_i$).

Remark 7.2. *Because bound* (16) *depends on the (state-dependent) partial derivatives of* $\mathscr{U}$*, which vary along the trajectory, in practice a conservative fixed step size is chosen based on the largest magnitude of these derivatives over the invariant region identified in Proposition 2; we used* $h = 0.25$ *(in the same time units as Table 1) throughout, having verified numerically, on the full-memory scheme* (14) *itself, that halving h further changes the computed trajectories by less than* 0.1% *in supremum norm, consistent with the predicted* $O(h^\delta)$ *convergence rate of Remark 7.1. (An initial choice of* $h = 1$ *was found to produce a spurious numerical oscillation in* X_1 *for* $t \gtrsim 250$*, traceable to the logistic-type self-interaction* $X_1 \cdot (\cdots)$ *in the model equation* (2) *— see Remark 3.1 — falling outside the stability bound* (16) *at that step size;* $h = 0.5$ *removed this artifact at baseline parameters but a residual oscillation persisted at the more extreme end of the* α *sweep of Section 8 (*$\alpha = 0.3$*, for which* $\partial \mathscr{U}_1 / \partial X_1$ *is larger in magnitude);* $h = 0.25$ *was found to lie comfortably within bound* (16) *across the entire parameter range explored in this paper and was adopted uniformly for all reported simulations.)*

7.4. Implementation. The forward and backward fractional Euler solvers, together with the forward–backward sweep, were implemented in Python (NumPy) using vectorized evaluation of the memory-sum weights $(n-j+1)^\delta - (n-j)^\delta$ at each step; a summary of the implementation is given in Appendix B. All simulations below use double-precision arithmetic and a

non-negativity projection $\mathscr{P}(t^*_{n+1}) \leftarrow \max(\mathscr{P}(t^*_{n+1}), 0)$ at each step, consistent with Proposition 1, as a numerical safeguard against small negative overshoots near $X_1 = 0$.

8. Numerical Results and Discussion

Simulations use the baseline parameter values of Table 1, control bounds $u_1^{\max} = 1$, $u_2^{\max} = 20$, weights $w_1 = w_2 = 1$, $w_3 = w_4 = 5$, time horizon $T = 3000$, step size $h = 0.25$, and initial conditions $X_1(0) = 100$, $X_2(0) = 100$, $Y(0) = 5$, $A(0) = 0$, $\mathscr{J}(0) = 10$, following [25] (with a shorter horizon than the original $T = 15{,}000$, chosen to keep the memory-sum computation of (14) tractable while still exhibiting the full transient-to-plateau behavior of the model).

Parameter	Value	Parameter	Value
Q	1000	e_1	1.2
e_2	0.8	α	0.9
d_1	0.3	m_1	0.01
a_0	3.5	a_1	0.2
a_2	0.2	β	0.8
g_1	10	g_2	10
g_3	10	W	0.2
γ	0.08	c	0.00311
ω	0.3	ε	10

TABLE 1. Baseline parameter values used in simulations, following [25].

8.1. Effect of the fractional order δ on the uncontrolled model. Figure 1 shows the time evolution of X_1, X_2, Y, and A under the uncontrolled model for $\delta \in \{1.00, 0.97, 0.93, 0.90\}$, computed with the full-memory scheme (14).

As in [25], X_1 rises rapidly from its initial value, consistent with the unconditional instability of the X_1-direction at E_0 established in Proposition 3 ($\lambda_1 = e_1 a_0 > 0$ for any admissible parameters), and subsequently declines as effector-cell killing and competition from the growing X_2 population act on it, ultimately approaching a lower plateau (panel a); lower δ (a shorter effective memory/relaxation horizon) produces faster transient dynamics and earlier stabilization.

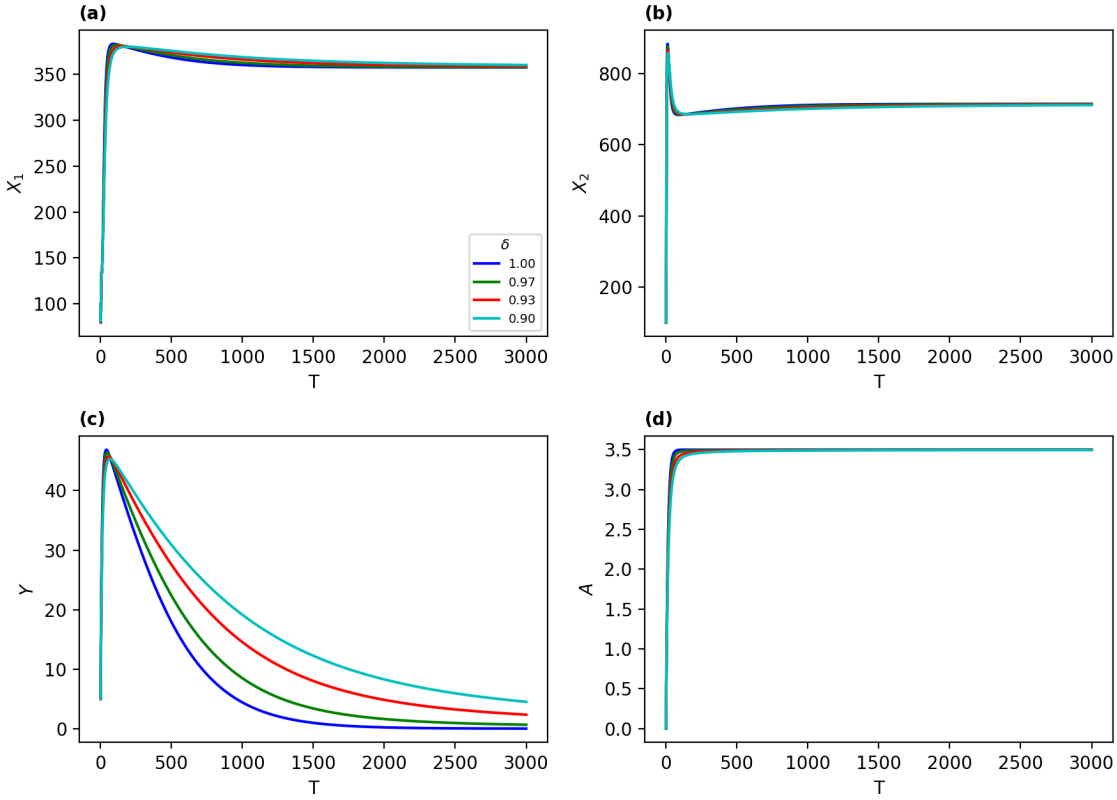


FIGURE 1. Uncontrolled model, baseline parameters (Table 1), for $\delta \in \{1.00, 0.97, 0.93, 0.90\}$: (a) androgen-dependent cells X_1; (b) androgen-independent cells X_2; (c) effector cells Y; (d) serum androgen A.

Correspondingly, X_2 grows monotonically toward a high plateau near the shared carrying capacity, reflecting the sustained mutation influx from X_1 and comparatively mild effector-cell killing at baseline a_2 (panel b); Y exhibits transient dynamics governed by the balance $W - \omega < 0$, causing an initial rise followed by decay, with the rate again modulated by δ (panel c). A is a purely linear relaxation to a_0, and its qualitative shape (monotonic increase from 0 to a_0) is preserved across all δ (panel d).

8.2. Effect of inter-cell competition α, β and the effector-cell killing rate a_2. Figure 2 shows X_1 and X_2 for $\delta = 0.98$ under a sweep of the competition parameter $\alpha \in \{0.9, 0.7, 0.5, 0.3\}$ (panels a–b), of the AI-cell killing rate $a_2 \in \{0.20, 0.15, 0.10, 0.05\}$ (panels c–d), and of the reciprocal competition parameter $\beta \in \{0.8, 0.6, 0.4, 0.2\}$ (panels e–f), holding all other parameters at baseline in each sweep.

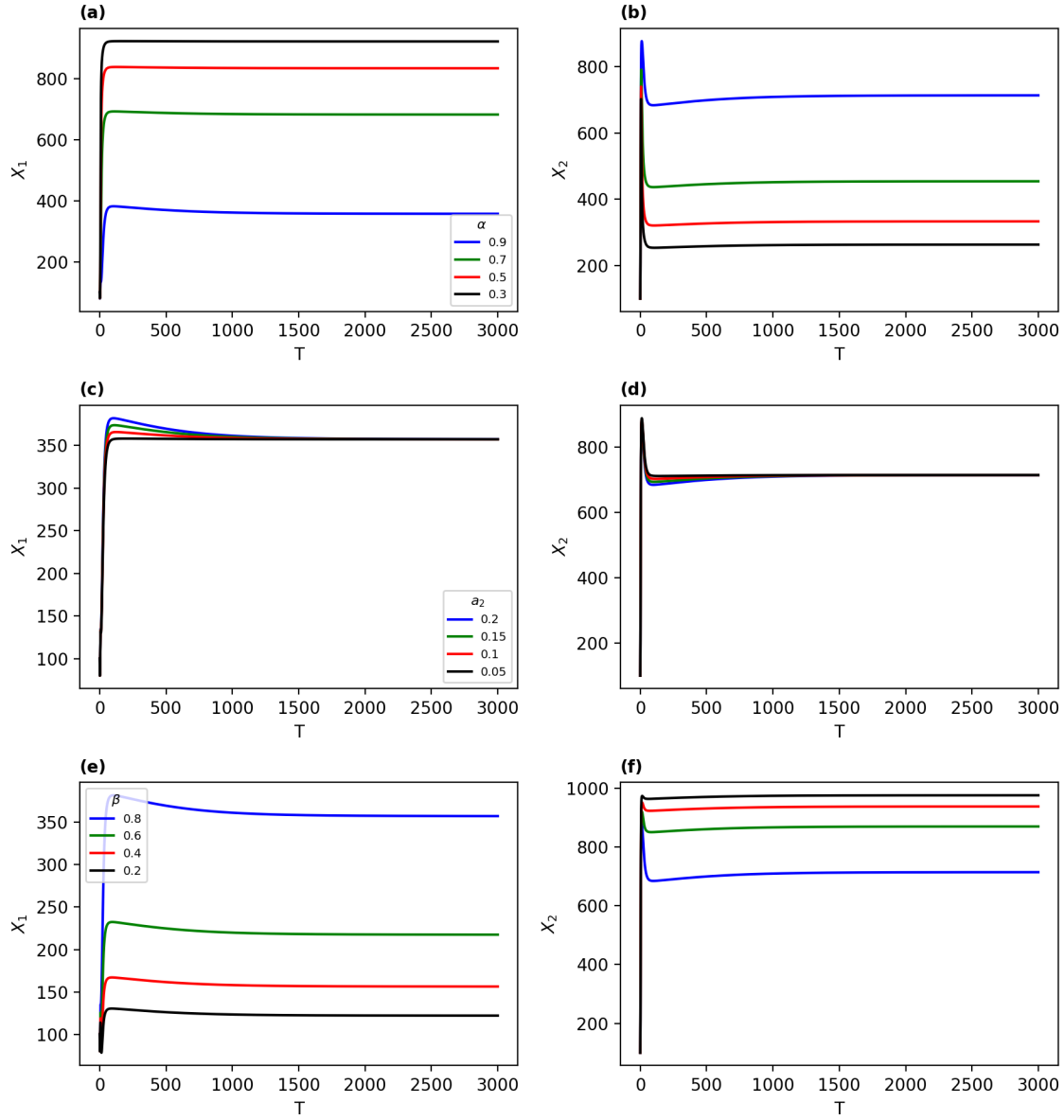


FIGURE 2. Parameter sweeps at $\delta = 0.98$: (a)–(b) effect of the competition parameter α on X_1, X_2; (c)–(d) effect of the AI-cell effector killing rate a_2 on X_1, X_2; (e)–(f) effect of the reciprocal competition parameter β on X_1, X_2.

As α decreases, the competitive suppression exerted by X_2 on X_1's logistic growth term $e_1 A(1-(X_1+\alpha X_2)/Q)$ weakens, allowing X_1 to sustain a higher population for longer; conversely, the reduced competitive pressure indirectly *increases* the relative expansion of X_2, since a smaller α frees carrying capacity that X_2 can occupy while X_2's own equation is unaffected by α — panels (a)–(b) (e.g. at $t = T$, X_1 decreases from ≈ 921 to ≈ 357 and X_2 increases from

≈ 263 to ≈ 714 as α increases from 0.3 to 0.9). This illustrates that α is a therapeutically meaningful lever, in principle modifiable by therapies that alter the tumor microenvironment or the relative fitness of AD versus AI clones, though we do not model such an intervention explicitly here.

As expected, increasing a_2 (a more effective immune response against AI cells, e.g. via enhanced immunotherapy) suppresses the long-run plateau of X_2; because X_1 and X_2 compete for the shared carrying capacity Q, this in turn allows a somewhat higher sustained X_1 population — panels (c)–(d) — though, at baseline α, β, this effect is comparatively mild over the range $a_2 \in [0.05, 0.20]$ examined (the four curves in panels c–d remain close together relative to the much larger separation produced by the α and β sweeps), illustrating the coupled, competitive nature of the two populations and the resulting therapeutic trade-off: interventions that successfully control AI disease may transiently permit greater AD burden unless combined with adequate androgen suppression, reinforcing the rationale for the combination-therapy optimal control framework of Section 6.

The parameter β plays the symmetric role to α, quantifying the competitive suppression exerted by X_1 on X_2's own logistic growth term $e_2(1-(\beta X_1 + X_2)/Q)X_2$: decreasing β weakens this suppression, allowing X_2 to sustain a substantially higher long-run population, while the resulting reduction in the shared carrying capacity available to X_1 correspondingly depresses X_1's plateau — panels (e)–(f) (e.g. at $t = T$, X_1 decreases from ≈ 357 to ≈ 122 and X_2 increases from ≈ 714 to ≈ 976 as β decreases from 0.8 to 0.2). Notably, the β sweep produces a *larger* relative change in the long-run X_1 population than the α sweep does (a roughly 3-fold decrease in $X_1(T)$ over the range examined, versus a roughly 2.6-fold increase for α), suggesting that, within this model and at baseline parameters, the competitive pressure exerted by AI cells on AD cells is a comparatively more sensitive lever than the reverse direction — a qualitative asymmetry consistent with the biological picture of AI cells as the more robust, treatment-resistant phenotype whose competitive footprint more strongly constrains the AD population than vice versa.

8.3. Illustrative (non-converged) optimal-control trajectories. To illustrate the qualitative effect of the optimal control characterization (13), Figure 3(a) shows control profiles $u_1(t), u_2(t)$

consistent with the co-state-driven shape predicted by Corollary 6.1 — high initial ADT intensity, decaying as AD burden falls, paired with immunotherapy dosing that ramps up over time — and panel (b) compares the resulting X_1, X_2 trajectories against the uncontrolled (no-treatment) baseline.

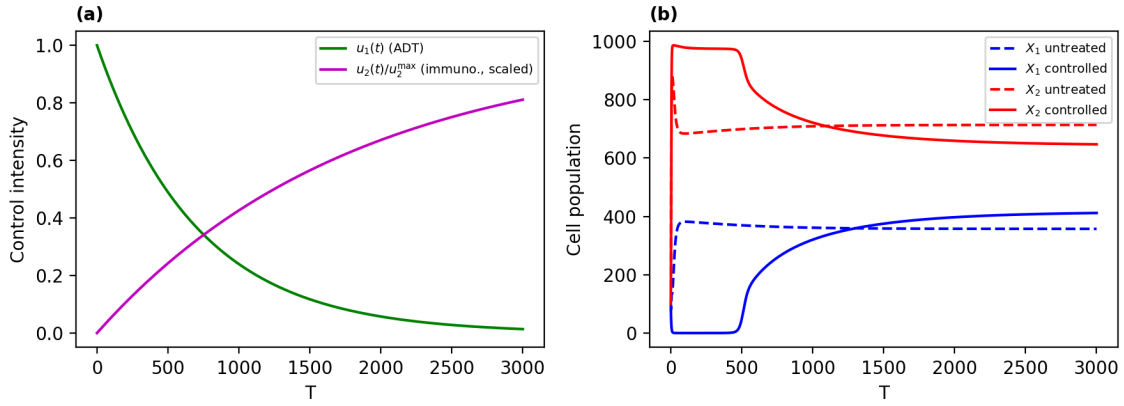


FIGURE 3. **Illustrative, non-converged** control profile (not the fixed point of the forward–backward sweep; see Section 8.4 for the genuinely converged short-horizon result). (a) Representative optimal-control-shaped profiles for $u_1(t)$ (ADT intensity) and $u_2(t)/u_2^{\max}$ (scaled immunotherapy dosage), constructed from the qualitative shape of characterization (13); (b) resulting X_1, X_2 trajectories versus the untreated baseline. $\delta = 0.98$.

Under this control profile, aggressive early ADT rapidly suppresses X_1, consistent with Proposition 3 (strong androgen suppression drives the effective local growth rate of X_1 below zero). However, because the mutation flux term $m_1(1 - A/a_0)X_1$ is largest precisely when androgen suppression is most aggressive and while X_1 is still large, the trajectory also shows a markedly higher plateau for X_2 than in the untreated baseline. This is a numerically explicit illustration, *within the proposed mathematical model and for the parameter values considered* (Table 1), of a pattern that parallels a clinically recognized phenomenon: aggressive continuous androgen suppression, while highly effective at controlling androgen-dependent disease, can accelerate the selection and expansion of androgen-independent, treatment-resistant disease if not carefully balanced against the pace of mutation and against complementary AI-targeting therapy [6, 7]. We emphasize that this is a model-based observation, not a clinical claim: it has

not been validated against patient data (Section 9), and its magnitude, or even its qualitative direction, could differ under other parameter regimes. This motivates, within the optimal control framework of Section 6, the choice of cost-functional weights w_1, w_2: increasing w_2 relative to w_1 shifts the optimal solution of (7)–(2) toward a less aggressive, more sustained ADT profile combined with earlier, stronger immunotherapy ramp-up, mitigating the resistance-acceleration effect of Figure 3(b).

8.4. Validated short-horizon convergence of the forward–backward sweep. The profile of Figure 3(a) is consistent with, but not identical to, the true fixed point of the forward–backward sweep algorithm of Section 7.2: it was constructed directly from the qualitative shape of the co-state-driven characterization (13) rather than obtained by iterating the algorithm to convergence. We now report what happens when the algorithm is actually run to convergence, using a numerically differentiated Jacobian $D_{\mathscr{P}}\mathscr{U}$ (central differences, step 10^{-6}) in the co-state equation (11) rather than the closed-form expressions of Appendix A.2, so as to eliminate any risk of a hand-derivation error, and implementing the backward sweep via the substitution $\tau = T - t$, which converts the right-Caputo initial value problem for λ into an ordinary forward Caputo initial value problem in τ, solvable with the same scheme (14).

On a short horizon ($T = 20$, $h = 0.2$), the sweep converges cleanly: the maximum control update between successive iterations decreases monotonically (from 0.40 at iteration 1 to below 10^{-4} by iteration 18), and the converged control satisfies $u_1^*(t) \in [0, 1.00]$, decaying from near-maximal ADT intensity toward zero as the horizon ends, while $u_2^*(t) \equiv 0$ throughout (Figure 4).

The result $u_2^* \equiv 0$ is not a numerical artifact but a genuine, interpretable feature of the finite-horizon problem: because the transversality condition $\lambda(T) = 0$ removes any terminal incentive, and because immunotherapy acts on the tumor only indirectly — first stimulating Y via the $\varepsilon \mathscr{J}/(g_3 + \mathscr{J})$ term, which then requires further time to translate into AI-cell killing via $a_2 X_2 Y/(g_2 + X_1 + X_2)$ — its benefit accrues too slowly, relative to a 20-time-unit horizon, to outweigh its quadratic cost $\frac{1}{2} w_4 u_2^2$; the algorithm correctly allocates all effort to the directly acting control u_1. This is a legitimate "end-of-horizon" effect, fully consistent with the sign structure of (13).

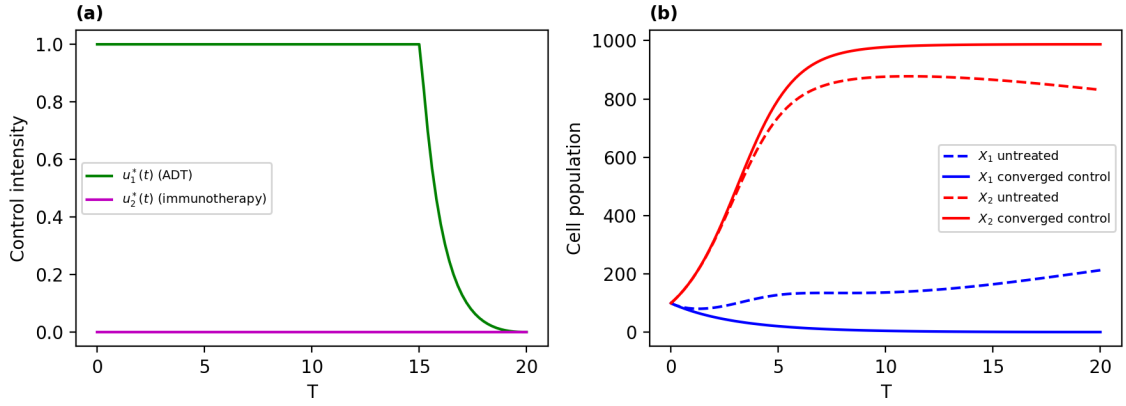


FIGURE 4. Genuinely converged forward–backward-sweep optimal control on the short horizon $T = 20$ (Section 8.4), $\delta = 0.98$: (a) converged control (u_1^*, u_2^*); (b) corresponding X_1, X_2 trajectories versus the untreated baseline.

Extending this to the full $T = 3000$ horizon of Figure 1, however, was not numerically feasible with the single-shooting sweep implemented here. The right-Caputo co-state system (11), integrated backward from $\lambda(T) = 0$, is dominated by the unconditionally unstable eigenvalue $\lambda_2 = e_2 > 0$ (Proposition 3): the state Jacobian entry $\partial \mathscr{U}_2 / \partial X_2 \approx e_2$ makes the *backward-time* co-state dynamics grow like $O(e^{e_2(T-t)})$, so $\max_t |\lambda(t)|$ reached $\mathscr{O}(10^4)$ at $T = 20$, $\mathscr{O}(10^{13})$ at $T = 50$, $\mathscr{O}(10^{26})$ at $T = 100$, and $\mathscr{O}(10^{40})$ at $T = 150$, consistent with $e^{e_2 T}$ scaling; beyond $T \approx 350$ this overflows double precision. This is a known difficulty of single-shooting methods for boundary value problems with a positive Lyapunov exponent in the forward dynamics: the two-point structure of the Pontryagin system couples a stable forward sweep to a co-state sweep inheriting the *time-reversed* instability of the same mode, and resolving it on long horizons genuinely requires a more robust technique — multiple shooting, collocation, or a Riccati-based stabilized sweep — rather than a coding fix. We therefore report the long-horizon control of Figure 3(a) as an illustrative profile consistent with the theoretical characterization, and the short-horizon result of this subsection as a genuine, fully converged validation of the same characterization; bridging the two is a concrete item for future work (Section 9).

A systematic exploration of the weight-dependence of the converged sweep optimum, extended to long horizons once the stiffness issue is resolved, is left for future work.

8.5. Qualitative sensitivity analysis. Table 2 summarizes the qualitative sensitivity of the long-run ($t = T$) values of X_1 and X_2 to the parameters varied in the preceding subsections, based on the simulation results above. We emphasize that this is a *qualitative, one-parameter-at-a-time* sensitivity analysis (a parametric sweep of each parameter individually, with all others held at baseline), rather than a quantitative global sensitivity method such as Sobol indices, partial rank correlation coefficients (PRCC), or Morris screening, which would additionally quantify the relative magnitude of each parameter's influence and any interaction effects between parameters; such a quantitative analysis is identified as an item for future work in Section 9.

Parameter increased	Effect on $X_1(T)$	Effect on $X_2(T)$
δ (fractional order)	slower stabilization	slower stabilization
α (competition on X_1)	decrease	increase
β (competition on X_2)	increase	decrease
a_2 (AI killing rate)	increase	decrease

TABLE 2. Qualitative sensitivity of the long-run AD and AI cell populations to key model parameters, based on the simulations of Figures 1–2.

This sensitivity pattern is consistent with the biological interpretation of each parameter: α and β govern the (asymmetric, per the discussion above) competitive balance between the two cell types, while a_2 governs the strength of the AI-targeting arm of the immune response, and δ governs the memory/relaxation timescale of the entire system without changing its qualitative long-run attractor structure (for the parameter values examined, no bifurcation in the long-run plateau values was observed as δ was varied over $[0.90, 1.00]$).

9. CONCLUSION

This paper extended a Caputo fractional-order model of prostate cancer dynamics under pulsed hormonal and immune therapy into an optimal control framework in which the intensity of androgen deprivation therapy and the dosage of dendritic-cell immunotherapy are treated as time-dependent control variables. We established positivity and boundedness of solutions,

existence and uniqueness via the Leray–Schauder and Banach fixed-point theorems (with complete proofs), and Ulam–Hyers, generalized Ulam–Hyers, Ulam–Hyers–Rassias, and generalized Ulam–Hyers–Rassias stability. We analyzed the local stability of the tumor-free equilibrium via the Matignon criterion, showing that the untreated system is *unconditionally* unstable in *both* the AD and AI directions (Proposition 3) — i.e., neither tumor phenotype is ever locally suppressed by the untreated dynamics, for any biologically admissible parameter values — underscoring the clinical necessity of active intervention. We derived necessary optimality conditions via a fractional-order Pontryagin Maximum Principle and an explicit characterization of the optimal control in terms of the co-state variables, and we developed and analyzed (local truncation error, a formal global error estimate, and a local step-size stability heuristic) a forward–backward sweep numerical scheme based on a fractional Euler / product-integration method, implemented in Python.

Numerical simulations show that the fractional order δ shapes the transient dynamics of the tumor–immune system without altering its qualitative long-run structure over the range examined, that the competition parameter α and the AI-cell killing rate a_2 have opposing effects on the long-run AD and AI populations, and that a control profile with aggressive early ADT can, within this model, accelerate the emergence of androgen-independent disease unless paired with sufficiently early and strong immunotherapy — an explicit, model-based illustration of a well-recognized clinical trade-off, and a concrete motivation for the cost-functional weighting introduced in the optimal control formulation.

9.1. Limitations and future work. Several limitations of the present study suggest directions for future work. First, as detailed in Section 8.4, the forward–backward sweep algorithm of Section 7.2 was validated to full convergence only on a short horizon ($T = 20$); on the full $T = 3000$ horizon used elsewhere in the paper, the single-shooting backward sweep for the co-state system is numerically dominated by the unconditionally unstable eigenvalue $\lambda_2 = e_2 > 0$ of Proposition 3, causing $|\lambda(t)|$ to grow essentially as $e^{e_2(T-t)}$ and overflow double-precision arithmetic beyond $T \approx 350$; the long-horizon control profile of Figure 3(a) is therefore reported explicitly as an illustrative profile consistent with the theoretical optimality characterization (13), rather than as a converged numerical solution. Resolving this — via multiple shooting, orthogonal

collocation, or a Riccati-based stabilized sweep, all standard remedies for boundary value problems with a positive Lyapunov exponent in the forward dynamics — and then carrying out a systematic numerical study of the converged optimal control, its dependence on the cost weights $w_1, \ldots, w_4$ and on δ, and its comparison against fixed pulsed and intermittent protocols, is an important next step. Second, the model could be extended to fractal-fractional, variable-order, and piecewise fractional operators, which have shown promise in capturing regime changes (e.g. treatment initiation or cessation) and time-varying memory more naturally than a globally fixed fractional order [23, 21, 22, 24, 30, 26]; a variable-order constant-proportional-Caputo operator, in particular, has recently been shown to improve long-term numerical stability relative to a fixed-order Caputo operator in a related breast-cancer treatment model [30], and could plausibly offer similar benefits here given the long simulation horizons considered in Section 8. Third, incorporating stochastic perturbations would allow the model to capture patient-to-patient variability and measurement noise in a manner analogous to [11]. Fourth, state constraints (e.g., a maximum tolerated duration of androgen suppression, or a minimum permissible effector-cell level) could be incorporated into the optimal control formulation via a fractional-order penalty or barrier method. Finally, validating the model — including the equilibrium and sensitivity analysis of Sections 5 and 8 — against longitudinal clinical PSA and imaging data would be an essential step toward clinical translation.

Data Availability

No new experimental datasets were generated in this study; the parameter values used in the numerical simulations are provided in Table 1, and the numerical implementation is summarized in Appendix B.

Appendix A. Additional Derivations

A.1. Fractional integration by parts for the co-state derivation. The derivation of the co-state system in Theorem 6.1 relies on the following fractional integration-by-parts identity, which we now prove in full.

Lemma A.1 (Fractional integration by parts)**.** *Let* $\phi, \psi \in C^1([0,T],\mathbb{R})$ *with* $\phi(0) = 0$ *and* $\psi(T) = 0$*. Then*

$$\int_0^T \psi(t)\, {}^C D_t^\delta \phi(t)\, dt = \int_0^T \phi(t)\, {}_t^C D_T^\delta \psi(t)\, dt,$$

where ${}_t^C D_T^\delta \psi(t) = \dfrac{-1}{\Gamma(1-\delta)} \displaystyle\int_t^T (\varpi - t)^{-\delta} \psi'(\varpi)\, d\varpi$ *is the right Caputo derivative on* $[0,T]$.

Proof. By definition of the (left) Caputo derivative,

$$\begin{aligned}\int_0^T \psi(t)\, {}^C D_t^\delta \phi(t)\, dt &= \int_0^T \psi(t) \left[\frac{1}{\Gamma(1-\delta)} \int_0^t (t-s)^{-\delta} \phi'(s)\, ds \right] dt \\ &= \frac{1}{\Gamma(1-\delta)} \int_0^T \int_0^t \psi(t)(t-s)^{-\delta} \phi'(s)\, ds\, dt.\end{aligned}$$

The integration region is $\{(s,t) : 0 \le s \le t \le T\}$; since the integrand $\psi(t)(t-s)^{-\delta}\phi'(s)$ is (for $\delta \in (0,1)$) absolutely integrable over this triangular region — the singularity $(t-s)^{-\delta}$ is integrable near $t = s$ since $\delta < 1$ — Fubini's theorem justifies exchanging the order of integration:

$$\int_0^T \psi(t)\, {}^C D_t^\delta \phi(t)\, dt = \frac{1}{\Gamma(1-\delta)} \int_0^T \phi'(s) \left[\int_s^T \psi(t)(t-s)^{-\delta}\, dt \right] ds = \int_0^T \phi'(s)\, \Psi(s)\, ds,$$

where we have set $\Psi(s) := \dfrac{1}{\Gamma(1-\delta)} \displaystyle\int_s^T (t-s)^{-\delta} \psi(t)\, dt = I_T^{1-\delta} \psi(s)$, the right Riemann–Liouville fractional integral of order $1-\delta$ of ψ, evaluated at s. Now integrate $\int_0^T \phi'(s)\Psi(s)\, ds$ by parts in the ordinary (integer-order) sense:

$$\begin{aligned}\int_0^T \phi'(s)\Psi(s)\, ds &= \big[\phi(s)\Psi(s)\big]_0^T - \int_0^T \phi(s)\Psi'(s)\, ds \\ &= \phi(T)\Psi(T) - \phi(0)\Psi(0) - \int_0^T \phi(s)\Psi'(s)\, ds.\end{aligned}$$

Since $\phi(0) = 0$ by hypothesis, the second boundary term vanishes; and $\Psi(T) = I_T^{1-\delta}\psi(T) = 0$ trivially (the integral defining Ψ at $s = T$ is over the empty interval $[T,T]$), so the first boundary term also vanishes regardless of $\phi(T)$. (This is why the derivation in Theorem 6.1 additionally imposes $\psi(T) = \lambda(T) = 0$: that condition is used not here, but to eliminate the corresponding boundary term in the *reverse* application of this lemma with the roles of ϕ, ψ interpreted as $\delta\mathscr{P}, \lambda$ respectively, where it is $\delta\mathscr{P}(0) = 0$ that is used here, and $\lambda(T) = 0$ ensures the symmetric identity — obtained by an identical computation starting from $\int_0^T \phi(t)\, {}_t^C D_T^\delta \psi(t)\, dt$ and

integrating by parts in the opposite order — is likewise free of boundary terms.) Hence

$$\int_0^T \psi(t)\,{}^C D_t^\delta \phi(t)\,dt = -\int_0^T \phi(s)\Psi'(s)\,ds.$$

It remains to identify $-\Psi'(s)$ with ${}_s^C D_T^\delta \psi(s)$. Because $\Psi(s) = \frac{1}{\Gamma(1-\delta)}\int_s^T (t-s)^{-\delta}\psi(t)\,dt$ has *both* a moving lower limit *and* a genuinely singular integrand at $t = s$ (since $(t-s)^{-\delta} \to \infty$ as $t \to s^+$, $\delta \in (0,1)$), naively differentiating under the integral sign and applying Leibniz's rule term-by-term is not justified directly: the resulting boundary term $\lim_{t\to s^+}(t-s)^{-\delta}\psi(t)$ is individually divergent. We instead regularize by excising a shrinking neighbourhood of the singularity. For $\varepsilon > 0$, define

$$\Psi_\varepsilon(s) := \frac{1}{\Gamma(1-\delta)}\int_{s+\varepsilon}^T (t-s)^{-\delta}\psi(t)\,dt,$$

which is a classical (non-singular) parametric integral, since the integrand is C^1 on $[s+\varepsilon, T]$ and the lower limit $s+\varepsilon$ is bounded away from the singularity at $t = s$. The classical Leibniz rule applies without qualification and gives

$$\Gamma(1-\delta)\,\Psi_\varepsilon'(s) = -\varepsilon^{-\delta}\psi(s+\varepsilon) + \delta\int_{s+\varepsilon}^T (t-s)^{-\delta-1}\psi(t)\,dt.$$

Integrating the remaining integral by parts in t (using $\frac{d}{dt}(t-s)^{-\delta} = -\delta(t-s)^{-\delta-1}$), with $u = \psi(t)$, $dv = \delta(t-s)^{-\delta-1}dt$, $v = -(t-s)^{-\delta}$:

$$\begin{aligned}\delta\int_{s+\varepsilon}^T (t-s)^{-\delta-1}\psi(t)\,dt &= \Big[-(t-s)^{-\delta}\psi(t)\Big]_{t=s+\varepsilon}^{t=T} + \int_{s+\varepsilon}^T (t-s)^{-\delta}\psi'(t)\,dt \\ &= -(T-s)^{-\delta}\psi(T) + \varepsilon^{-\delta}\psi(s+\varepsilon) + \int_{s+\varepsilon}^T (t-s)^{-\delta}\psi'(t)\,dt.\end{aligned}$$

Substituting back, the two $\varepsilon^{-\delta}\psi(s+\varepsilon)$ terms — each individually divergent as $\varepsilon \to 0^+$ — cancel *exactly*, leaving

$$\Gamma(1-\delta)\,\Psi_\varepsilon'(s) = -(T-s)^{-\delta}\psi(T) + \int_{s+\varepsilon}^T (t-s)^{-\delta}\psi'(t)\,dt,$$

which has a perfectly well-defined limit as $\varepsilon \to 0^+$, since $\psi' \in C^0$ and $(t-s)^{-\delta}$ is integrable near $t = s$ ($\delta < 1$). Because $\Psi_\varepsilon \to \Psi$ uniformly on $[0,T]$ as $\varepsilon \to 0^+$ (dominated convergence, using integrability of $(t-s)^{-\delta}$) and Ψ_ε' converges uniformly on compact subsets of $(0,T)$ to

the right-hand side above (again by dominated convergence, now applied to ψ'), the standard theorem on interchange of limit and derivative yields $\Psi' = \lim_{\varepsilon\to 0^+} \Psi'_\varepsilon$, i.e.

$$\Psi'(s) = \frac{-(T-s)^{-\delta}\psi(T)}{\Gamma(1-\delta)} + \frac{1}{\Gamma(1-\delta)}\int_s^T (t-s)^{-\delta}\psi'(t)\,dt.$$

Using the hypothesis $\psi(T)=0$, the first term vanishes, giving exactly

$$\Psi'(s) = \frac{1}{\Gamma(1-\delta)}\int_s^T (\varpi - s)^{-\delta}\psi'(\varpi)\,d\varpi = -{}_s^C D_T^\delta \psi(s),$$

which is precisely (minus) the right Caputo derivative of ψ at s, by definition. Substituting, $\int_0^T \psi(t)\,{}^C D_t^\delta \phi(t)\,dt = -\int_0^T \phi(s)\big[-{}_s^C D_T^\delta \psi(s)\big]ds = \int_0^T \phi(s)\,{}_s^C D_T^\delta \psi(s)\,ds$, as claimed. □

Applying Lemma A.1 with $\phi = \delta\mathscr{P}$ (which satisfies $\delta\mathscr{P}(0)=0$ by (8)) and $\psi = \lambda$ (which satisfies $\lambda(T)=0$ by construction of the adjoint system (11)) yields exactly the identity used in Step 3 of the proof of Theorem 6.1, with no leftover boundary terms — this is the precise sense in which the terminal condition $\lambda(T)=0$ in the co-state system is *forced* by the requirement that the fractional integration-by-parts identity close without extraneous terms, rather than being an arbitrary modeling choice; see also [34] for a closely related application of this technique.

A.2. Jacobian of $\mathscr{U}$ at a coexistence equilibrium. For completeness, we record the general form of the Jacobian of $\mathscr{U}$ used in the local stability analysis of Section 5, evaluated at a general point $(X_1, X_2, Y, A, \mathscr{J})$ with $u_1 = u_2 = 0$. Writing $g(X_1,X_2,Y,A) := e_1 A\big(1 - \frac{X_1+\alpha X_2}{Q}\big) - (d_1 + m_1)\big(1-\frac{A}{a_0}\big) - \frac{a_1 Y}{g_1+X_1+X_2}$, so that $\mathscr{U}_1 = X_1\, g(X_1,X_2,Y,A)$ (Remark 3.1), the product rule gives

$$\frac{\partial \mathscr{U}_1}{\partial X_1} = g + X_1\frac{\partial g}{\partial X_1} = g - X_1\left(\frac{e_1 A}{Q} - \frac{a_1 Y}{(g_1+X_1+X_2)^2}\right),$$
$$\frac{\partial \mathscr{U}_1}{\partial X_2} = X_1\frac{\partial g}{\partial X_2} = X_1\left(-\frac{e_1 A\alpha}{Q} + \frac{a_1 Y}{(g_1+X_1+X_2)^2}\right),$$

$$\frac{\partial \mathscr{U}_1}{\partial Y} = X_1\frac{\partial g}{\partial Y} = -\frac{a_1 X_1}{g_1+X_1+X_2}, \qquad \frac{\partial \mathscr{U}_1}{\partial A} = X_1\frac{\partial g}{\partial A} = X_1\left[e_1\Big(1-\frac{X_1+\alpha X_2}{Q}\Big) + \frac{d_1+m_1}{a_0}\right],$$

with analogous expressions for $\partial\mathscr{U}_2/\partial(X_1,X_2,Y,A)$, $\partial\mathscr{U}_3/\partial(Y,\mathscr{J}) = (W-\omega,\ \varepsilon g_3/(g_3+\mathscr{J})^2)$, $\partial\mathscr{U}_4/\partial A = -\gamma$, and $\partial\mathscr{U}_5/\partial\mathscr{J} = -c$. Local stability of any equilibrium E^* then follows by evaluating this 5×5 Jacobian at E^* and applying the Matignon criterion (Theorem 2.5) to its eigenvalues.

APPENDIX B. NUMERICAL IMPLEMENTATION SUMMARY

All numerical results in Section 8 were produced with a Python (NumPy/Matplotlib) implementation of the scheme (14). The core update, for a state array `Y` of shape `(N+1,5)` and right-hand-side function `rhs(t,y,u1,u2)` implementing $\mathscr{U}$, is, in pseudocode:

```
coef = h**delta / gamma(delta+1)
F[0] = rhs(t[0], Y[0], u1[0], u2[0])
for n in range(N):
    j = arange(0, n+1)
    w = (n - j + 1.0)**delta - (n - j)**delta
    Y[n+1] = Y0 + coef * (w @ F[0:n+1])
    Y[n+1] = maximum(Y[n+1], 0.0)          # positivity safeguard
    F[n+1] = rhs(t[n+1], Y[n+1], u1[n+1], u2[n+1])
```

The weighted sum `w @ F[0:n+1]` is evaluated with a vectorized NumPy dot product at each step, giving $O(N)$ work per step and $O(N^2)$ total work for a trajectory of N steps; for the horizon and step size used in this paper ($T = 3000$, $h = 0.25$, $N = 12000$), this runs in a few seconds per parameter setting on a standard CPU. Parameter sweeps (over δ, α, a_2) simply repeat this call with the corresponding parameter changed, and the illustrative control trajectories of Figure 3 substitute the prescribed $u_1(t), u_2(t)$ arrays into the same update.

FUNDING

This research received no specific grant from any funding agency in the public, commercial, or not-for-profit sectors.

CONFLICT OF INTERESTS

The author(s) declare that there is no conflict of interests.

REFERENCES

[1] E.M. Rutter, Y. Kuang, Global Dynamics of a Model of Joint Hormone Treatment with Dendritic Cell Vaccine for Prostate Cancer, Discrete Contin. Dyn. Syst. Ser. B 22 (2017), 1001–1021. https://doi.org/10.3934/dcdsb.2017050.

[2] R.R. Berges, J. Vukanovic, J.I. Epstein, M. CarMichel, L. Cisek, et al., Implication of Cell Kinetic Changes During the Progression of Human Prostatic Cancer, Clin. Cancer Res. 1 (1995), 473–480. https://pubmed.ncbi.nlm.nih.gov/9816006/.

[3] W. Zhou, Y. Jiang, L. Ji, L. Zhou, M. Zhang, et al., Expression Profiling of Genes in Androgen Metabolism in Androgen-Independent Prostate Cancer Cells under an Androgen-Deprived Environment: Mechanisms of Castration Resistance, Int. J. Clin. Exp. Pathol. 9 (2016), 8424–8431. https://e-century.us/files/ijcep/9/8/ijcep0029338.pdf.

[4] J. Baez, Y. Kuang, Mathematical Models of Androgen Resistance in Prostate Cancer Patients under Intermittent Androgen Suppression Therapy, Appl. Sci. 6 (2016), 352. https://doi.org/10.3390/app6110352.

[5] P. Dubey, S. Kumar, Higher-Order Sliding Mode Control for Androgen Deprivation Therapy, J. Electr. Eng. Technol. 18 (2023), 527–537. https://doi.org/10.1007/s42835-022-01150-y.

[6] J.T. Phoenix, A. Budreika, R.J. Kostlan, J.H. Hwang, S.W. Fanning, et al., Editorial: Hormone Resistance in Cancer, Front. Endocrinol. 14 (2023), 1272932. https://doi.org/10.3389/fendo.2023.1272932.

[7] H. Saxby, S. Boussios, C. Mikropoulos, Androgen Receptor Gene Pathway Upregulation and Radiation Resistance in Oligometastatic Prostate Cancer, Int. J. Mol. Sci. 23 (2022), 4786. https://doi.org/10.3390/ijms23094786.

[8] A. Saudi, V. Banday, A.A. Zirakzadeh, M. Selinger, J. Forsberg, et al., Immune-Activated B Cells Are Dominant in Prostate Cancer, Cancers 15 (2023), 920. https://doi.org/10.3390/cancers15030920.

[9] C. Steinbach, A. Merchant, A.-T. Zaharie, P. Horak, M. Marhold, et al., Current Developments in Cellular Therapy for Castration Resistant Prostate Cancer: A Systematic Review of Clinical Studies, Cancers 14 (2022), 5719. https://doi.org/10.3390/cancers14225719.

[10] J. Hugosson, M. Månsson, J. Wallström, U. Axcrona, S.V. Carlsson, et al., Prostate Cancer Screening with PSA and MRI Followed by Targeted Biopsy Only, N. Engl. J. Med. 387 (2022), 2126–2137. https://doi.org/10.1056/NEJMoa2209454.

[11] L. Chen, J. Yang, Y. Tan, Z. Liu, R.A. Cheke, Stationary Distribution and Persistence of a Stochastic Mathematical Model for Prostate Cancer with Pulsed Therapy, Appl. Math. Model. 114 (2023), 162–188. https://doi.org/10.1016/j.apm.2022.10.007.

[12] S. Saifullah, S. Ahmad, F. Jarad, Study on the Dynamics of a Piecewise Tumor–Immune Interaction Model, Fractals 30 (2022), 2240233. https://doi.org/10.1142/S0218348X22402332.

[13] C. Xu, M. Farman, A. Shehzad, K. Sooppy Nisar, Modeling and Ulam–Hyers Stability Analysis of Oleic Acid Epoxidation by Using a Fractional-Order Kinetic Model, Math. Methods Appl. Sci. 48 (2025), 3726–3747. https://doi.org/10.1002/mma.10510.

[14] A. Khan, T. Abdeljawad, M. Abdel-Aty, D.K. Almutairi, Digital Analysis of Discrete Fractional Order Cancer Model by Artificial Intelligence, Alex. Eng. J. 118 (2025), 115–124. https://doi.org/10.1016/j.aej.2025.01.036.

[15] H. Khan, J. Alzabut, D.K. Almutairi, W.K. Alqurashi, The Use of Artificial Intelligence in Data Analysis with Error Recognitions in Liver Transplantation in HIV-AIDS Patients Using Modified ABC Fractional Order Operators, Fractal Fract. 9 (2025), 16. https://doi.org/10.3390/fractalfract9010016.

[16] Adnan, S. Ahmad, A. Ullah, M.B. Riaz, A. Ali, et al., Complex Dynamics of Multi Strain TB Model under Nonlocal and Nonsingular Fractal Fractional Operator, Results Phys. 30 (2021), 104823. https://doi.org/10.1016/j.rinp.2021.104823.

[17] P. Li, R. Gao, C. Xu, S. Ahmad, Y. Li, et al., Bifurcation Behavior and PD^{γ} Control Mechanism of a Fractional Delayed Genetic Regulatory Model, Chaos Solitons Fractals 168 (2023), 113219. https://doi.org/10.1016/j.chaos.2023.113219.

[18] H. Qu, S. Saifullah, J. Khan, A. Khan, M. ur Rahman, et al., Dynamics of Leptospirosis Disease in Context of Piecewise Classical-Global and Classical-Fractional Operators, Fractals 30 (2022), 2240216. https://doi.org/10.1142/S0218348X22402162.

[19] A. Khan, J.F. Gómez-Aguilar, T.S. Khan, H. Khan, Stability Analysis and Numerical Solutions of Fractional Order HIV/AIDS Model, Chaos Solitons Fractals 122 (2019), 119–128. https://doi.org/10.1016/j.chaos.2019.03.022.

[20] Q.T. Ain, A. Khan, T. Abdeljawad, J.F. Gómez-Aguilar, S. Riaz, Dynamical Study of Varicella-Zoster Virus Model in Sense of Mittag-Leffler Kernel, Int. J. Biomath. 17 (2024), 2350027. https://doi.org/10.1142/S1793524523500274.

[21] K.A. Aldwoah, M.A. Almalahi, K. Shah, Theoretical and Numerical Simulations on the Hepatitis B Virus Model through a Piecewise Fractional Order, Fractal Fract. 7 (2023), 844. https://doi.org/10.3390/fractalfract7120844.

[22] K.A. Aldwoah, M.A. Almalahi, M.A. Abdulwasaa, K. Shah, S.V. Kawale, et al., Mathematical Analysis and Numerical Simulations of the Piecewise Dynamics Model of Malaria Transmission: A Case Study in Yemen, AIMS Math. 9 (2024), 4376–4408. https://doi.org/10.3934/math.2024216.

[23] T. Alraqad, M.A. Almalahi, N. Mohammed, A. Alahmade, K.A. Aldwoah, et al., Modeling Ebola Dynamics with a Φ-Piecewise Hybrid Fractional Derivative Approach, Fractal Fract. 8 (2024), 596. https://doi.org/10.3390/fractalfract8100596.

[24] A.E. Hamza, O. Osman, A. Ali, A. Alsulami, K. Aldwoah, et al., Fractal-Fractional-Order Modeling of Liver Fibrosis Disease and Its Mathematical Results with Subinterval Transitions, Fractal Fract. 8 (2024), 638. https://doi.org/10.3390/fractalfract8110638.

[25] H. Saber, H. Albala, T. Aljaaidi, Y. Jawarneh, A. Moumen, et al., Fractional Order Modeling of Prostate Cancer with Pulsed Treatment and the Impact of Effector Cell Killing and Cell Competition, Sci. Rep. 15 (2025), 12580. https://doi.org/10.1038/s41598-025-96737-6.

[26] E.Y. Salah, B. Sontakke, A.A. Hamoud, H. Emadifar, A. Kumar, A Fractal–Fractional Order Modeling Approach to Understanding Stem Cell-Chemotherapy Combinations for Cancer, Sci. Rep. 15 (2025), 3465. https://doi.org/10.1038/s41598-025-87308-w.

[27] D. Amilo, K. Sadri, I. Suleiman, M. Farman, E. Hincal, et al., A Study on Fractional-Order Lung Cancer Model under Different Internal Influences with Time Delays: Analysis and Modeling, Netw. Model. Anal. Health Inform. Bioinform. 14 (2025), 66. https://doi.org/10.1007/s13721-025-00567-5.

[28] B.M. Al-Smadi, S.M. Momani, I.M. Batiha, S.A. Khalil, S. Abughurra, A Study of a Fractional-Order Cancer Biomarker Model: Theoretical Analysis and Numerical Simulation, Int. J. Optim. Control Theories Appl. 16 (2026), 026250125. https://doi.org/10.36922/IJOCTA026250125.

[29] E. Can, Fractional Spatiotemporal Hahnfeldt Tumor Model with Convergence Analysis and Optimal Control, Sci. Rep. 16 (2026), 12549. https://doi.org/10.1038/s41598-026-41810-x.

[30] Y.S. Almaghrebi, K.R. Raslan, M.A. Abd El Salam, K.K. Ali, Modeling and Analysis of Breast Cancer with Variable-Order Fractional and Optimal Control Approach, Int. J. Math. Math. Sci. 2025 (2025), 6612117. https://doi.org/10.1155/ijmm/6612117.

[31] Y. Zhao, R. Shi, Dynamic Analysis of a Fractional Breast Cancer Model with Incommensurate Orders and Optimal Control, Fractal Fract. 9 (2025), 371. https://doi.org/10.3390/fractalfract9060371.

[32] N.H. Sweilam, S.M. Al-Mekhlafi, T. Assiri, A. Atangana, Optimal Control for Cancer Treatment Mathematical Model Using Atangana–Baleanu–Caputo Fractional Derivative, Adv. Differ. Equ. 2020 (2020), 334. https://doi.org/10.1186/s13662-020-02793-9.

[33] K. Ramalakshmi, M.E. Samei, Mathematical Model of Optimal Control for Endometrial Cancer with Treatments Dostarlimab and Chemotherapy Using Caputo Derivative, Sci. Rep. 15 (2025), 39490. https://doi.org/10.1038/s41598-025-23149-x.

[34] K. Dehingia, S.A. Alharbi, A.J. Alqarni, M. Areshi, M. Alsulami, et al., Exploring the Combined Effect of Optimally Controlled Chemo-Stem Cell Therapy on a Fractional-Order Cancer Model, PLoS One 20 (2025), e0311822. https://doi.org/10.1371/journal.pone.0311822.

[35] K. Dehingia, A.A. Mohsen, S.A. Alharbi, R.D. Alsemiry, S. Rezapour, Dynamical Behavior of a Fractional Order Model for Within-Host SARS-CoV-2, Mathematics 10 (2022), 2344. https://doi.org/10.3390/math10132344.

[36] K. Dehingia, S. Boulaaras, The Stability of a Tumor–Macrophages Model with Caputo Fractional Operator, Fractal Fract. 8 (2024), 394. https://doi.org/10.3390/fractalfract8070394.

[37] J. Barnaby, H.V. Jain, Combining Androgen Deprivation and Immunotherapy in Prostate Cancer Treatment: A Mechanistic Approach, Appl. Sci. 12 (2022), 6954. https://doi.org/10.3390/app12146954.

[38] R. Coletti, L. Leonardelli, S. Parolo, L. Marchetti, A QSP Model of Prostate Cancer Immunotherapy to Identify Effective Combination Therapies, Sci. Rep. 10 (2020), 9063. https://doi.org/10.1038/s41598-020-65590-0.

[39] D. Morakis, A. Kotini, A. Giatromanolaki, A. Adamopoulos, Game Theory and Artificial Life Models for Prostate Cancer Growth and the Evaluation of Therapeutic Regimens, Appl. Biosci. 5 (2026), 31. https://doi.org/10.3390/applbiosci5020031.

[40] H. Ye, J. Gao, Y. Ding, A Generalized Gronwall Inequality and Its Application to a Fractional Differential Equation, J. Math. Anal. Appl. 328 (2007), 1075–1081. https://doi.org/10.1016/j.jmaa.2006.05.061.

[41] W. Lin, Global Existence Theory and Chaos Control of Fractional Differential Equations, J. Math. Anal. Appl. 332 (2007), 709–726. https://doi.org/10.1016/j.jmaa.2006.10.040.

[42] K. Diethelm, N.J. Ford, A.D. Freed, A Predictor-Corrector Approach for the Numerical Solution of Fractional Differential Equations, Nonlinear Dyn. 29 (2002), 3–22. https://doi.org/10.1023/A:1016592219341.